UNIUNEA EUROPEANĂ

Fondul Social European
POSDRU 2007-2013

Instrumente Structurale
2007-2013

OIPOSDRU

MINISTERUL EDUCAȚIEI ȘI CERCETĂRII ȘTIINȚIFICE

Universitatea POLITEHNICA din București

University POLITEHNICA of Bucharest

Doctoral School of Industrial Engineering and Robotics

University of Pitesti

Interdisciplinary Doctoral School

Eng. CONSTANTIN G. Marius-Adrian

PhD THESIS

Summary

Contributions to the development on friction stir welding processes and systems with rotating active element and additional heat input of copper structures

Scientific Supervisors,

Prof. univ. dr. eng. Marian GHEORGHE

Prof. univ. dr. eng. Eduard Laurențiu NIȚU

- 2020 -

Table of contents

Keywords

friction stir welding,
copper,
process temperature,
axial process force,
roughness,
macrostructure,
microstructure,
microhardness,
tensile strength,
numerical modeling.

Foreword

Research and development of friction stir welding processes and systems with rotating active element without or with additional heat input, FSW, respectively, FSW-TIG, in order to determine the technological conditions of welding for some copper structures, represents the motivation and direction of doctoral studies, completed by this doctoral thesis.

The doctoral program consisted of taking exams, preparing and presenting scientific reports, deepening the study, proposing and developing a research methodology, conducting experimental research, data processing and analysis of dependency relationships to determine FSW and FSW-TIG welding conditions of target structures at acceptable levels of their characteristics and productivity, proposal and development of a numerical model for processes simulation, realization and publication of scientific papers, as well as elaboration of the present doctoral thesis on friction stir welding processes with rotating active element without or with additional heat input, FSW, respectively, FSW-TIG.

I would like to extend my deepest thanks to Prof.univ.dr.eng. Marian GHEORGHE and Prof.univ.dr.eng. Eduard Laurențiu NIȚU, for the scientific guidance and coordination of the entire activity of completing the doctoral program, the support, full confidence and total availability granted during this period.

I sincerely thank Eng. Radu COJOCARU and Eng. Cristi CIUCĂ from the "National Research and Development Institute for Welding and Material Testing" - ISIM Timisoara, for their support in making welded joints.

I express my deepest thanks to Conf.dr.eng. Claudiu BĂDULESCU from ENSTA Bretagne, under whose guidance Eng. Diana SCIRLOI and Dr.fiz. Denis NEGREA contributed to the determination of some mechanical properties of the joints.

I express my sincere thanks to Prof.univ.dr.eng. Nicolae IONESCU and Prof.univ.dr.eng. Tom SAVU - from POLITEHNICA University of Bucharest, Conf.univ.dr.eng. Daniela Monica IORDACHE - from University of Pitesti and Dr.eng. CSP 1 Gheorghe POPAN - from the National Institute of Research and Development in Mechatronics and Measurement Technique - Bucharest, for the comments and recommendations addressed within the Commission for evaluation and public presentation of the doctoral thesis.

I am grateful to my family, job colleagues and PhD colleague Eng. Ana BOȘNEAG for the moral support and understanding shown during the doctoral studies.

The activities within the doctoral studies took place at POLITEHNICA University of Bucharest and University of Pitesti, according to the Doctoral Collaboration Agreement concluded between the two institutions. Also, some of the activities regarding the elaboration of this doctoral thesis benefited from the support of the Sectoral Operational Program for Human Resources Development (POSDRU), financed by the European Social Fund and the Government of Romania, through contract no. POSDRU/187/1.5/ S/155536.

Marius Adrian CONSTANTIN

Introduction

Copper and its alloys present specific properties - electrical and thermal conductivity, ductility, tensile strength, corrosion resistance - and are used in various industrial applications. But these materials are difficult to weld by fusion welding technologies due to their high thermal conductivity and high rate of oxidation at temperatures very close to the melting temperature. Within the welding technologies of copper and its alloys, friction stir welding processes with rotating active element without or with additional heat input, FSW, respectively, FSW-TIG, are also developed.

The friction stir welding process with rotating active element, FSW, is a solid state welding process based on the heat generated by friction and plastic deformation performed at the interaction between a rotating active element and the parts to be welded. The friction stir welding process with rotating active element assisted by a TIG (Tungsten Inert Gas) equipment in order to generate additional heat input in the process, represents the hybrid FSW-TIG process.

* * *

In the first part of this doctoral thesis, based on the analysis of the current state of research and development of friction stir welding processes and systems with rotating active element without or with additional heat input, relevant data are presented - types of processes, principles and technological parameters, characteristics of the rotating active element, characteristics of technological equipment, industrial applications, process characteristics, characteristics of welded structures, numerical modeling and simulation of processes, conclusions.

In the second part of the doctoral thesis, based on the data and conclusions drawn from the analysis of the current state, are formulated the directions and main objective of the research and development activity within the doctorate - development, through theoretical-experimental research and numerical modeling, of friction stir welding processes and systems with rotating active element without or with additional heat input of some copper structures.

Next, reference methodological elements are defined and, in relation to them, are performed preliminary and advanced theoretical-experimental researches on friction stir welding processes with rotating active element without or with additional heat input, FSW, respectively, FSW-TIG of some structures consisting of two Cu-DHP plates positioned side by side, the preliminary research - to determine the main states and trends of the characteristics and dependency relations and the advanced research - to validate or determine defining characteristics and dependency relations, respectively, FSW and FSW-TIG welding conditions of Cu-DHP structures at acceptable levels of their characteristics and productivity. In essence: after planning and preparing all the elements and the technological welding system, at each planned experiment - defined by a certain combination of values of the rotational speed, welding speed and TIG source intensity - the axial process force and process temperature are measured, continuously, during the working period in which the welded structure is made; the data are processed and the dependency relations between the involved scales are analyzed as appropriate; the planned specimens are sampled and prepared; important elements for defining the characteristics of welded structures are determined - macrostructure, microstructure, microhardness, roughness, tensile strength, percentage total extension at fracture; the data are processed and the dependency relations between the involved scales are analyzed as appropriate; an analysis of the defects inside the welded joints is performed by tensile testing and digital image correlation. Also, a thermomechanical coupled three-dimensional numerical model of the FSW process is developed, through which it is simulated the FSW process, determining the process temperature distribution in accordance with the experimental results, studied and shown that in order reduce the computational time of the numerical simulation, mass scaling is efficient and acceptable in accuracy.

The final conclusions and the main contributions brought by this doctoral thesis to the development and numerical modeling of friction stir welding processes and systems with rotating active element without or with additional heat input of some Cu-DHP structures, scientific and practical importance of the doctoral thesis, as well as perspectives - continuous and analytical development on the technical-economic characteristics, modeling and simulation, industrial implementation, at higher levels of evaluation indicators are presented.

Part I.

Current state of research and development of friction stir welding processes and systems with rotating active element without or with additional heat input

Chapter 1. Friction stir welding processes with rotating active element without or with additional heat input

1.1. Welding copper and its alloys

Copper and copper based alloys offer unique combinations of electrical and thermal conductivity, mechanical strength, formability and corrosion resistance and are used in a wide range of engineering applications. Other valuable attributes of these materials include color, spark resistance, and nonmagnetic behavior. Different types of copper alloys are used in industry, of which the most common are: brass, bronze, red brass, nickel copper alloys, silver-nickel alloys and beryllium copper alloys.

In industry, the joining of copper and copper based alloys is usually done by various melt welding processes, solder joining processes and solid-state welding processes. The main factors affecting the weldability of copper and its alloys by fusion welding processes are [B06]:

• The effect of thermal conductivity, which requires the use of high intensities of heat sources to obtain localized melting in pure copper and its alloys.
• The welding position mainly used is the horizontal one, considering the extremely fluid nature of these materials, the vertical positioning or overlapping of the parts being used very rarely.
• The high coefficient of thermal expansion causes an increase in shrinkage forces during the solidification of copper alloys, which causes hot cracking.
• Presence of porosity caused by vaporization of alloying elements with low melting temperature.
• The need to use a protective gas imposed by the tendency of these materials to absorb gases from the air, which causes the formation of pores and cracks.
• Cleaning and protecting surfaces to prevent the formation of oxides.
• The presence of alloying elements that are both volatile and toxic.

Copper brazing and soldering are sometimes preferred techniques to avoid problems that may be associated with melt welding processes, but the mechanical strength of these joints is usually lower than the strength of joints obtained by other welding processes [M12].

Another way to avoid the problems associated with melt welding processes is to use solid state welding. A friction welding process, which is suitable for this type of material, is the friction welding process with rotating active element, FSW [M13, NO2]. This process is able to produce in pure copper thick welds, with mechanical properties superior to melt welding, in a reliable and reproducible way [M12, S05].

1.2. Friction stir welding process

Friction stir welding process, FSW, is a solid-state welding process invented by Thomas and his collaborators in 1991 [T02]. This technology was originally used for welding aluminum alloys from groups classified as non-weldable using conventional melting welding techniques, but over time has also focused on other materials such as copper, magnesium, titanium, steel, polymeric or composite materials [B07, B14, L02, M11].

Friction stir welding (FSW) is a solid-state joining process based on the heat generated by friction and plastic deformation by a non-consumable welding tool, called an active element, when interacting with the parts to be joined. The active element that performs a rotational movement around its own axis, penetrates transversely into the parts to be joined, after which a translational movement is performed in the direction of the joint line. The plasticized material is transferred behind it, thus forming the welded joint (Fig. 1.2.1) [D06, J06, L02].

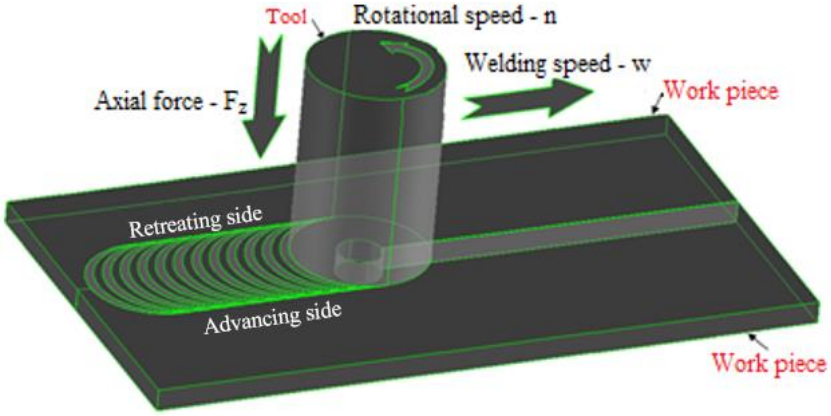

Fig. 1.2.1. Schematic presentation of the FSW welding process

The FSW welding process consists of four stages, namely: penetration, maintenance, effective welding, retraction [C06, F01, L02]. The FSW weld bead is not symmetrical in relation to the joint line, this asymmetry being due to the process kinematics [G03]. Thus, according to ISO/DIS 25239-3, an FSW joint consists of two sides, an advancing side and a retracting side.

The technological parameters characteristic of the FSW process are related to the positioning of the active element and to the movements it performs during the welding process, respectively: its rotational speed [rpm] - n, welding speed [mm/min] - w, the applied axial force [kN] - F_z and the tool tilt angle [º] - α (Fig. 2.2.1).

1.3. Advantages and disadvantages of friction stir welding process

Due to its solid nature, the friction stir welding process, FSW, has many advantages compared to conventional melting welding processes, such as:

1. Its ability to weld alloys of materials that are non-weldable or difficult to weld using fusion welding techniques, as well as alloys of different materials [D04, K03, K07];
2. Eliminates the problems associated with fusion welding processes, because this process is performed without melting the material [A04, B05, H04];
3. Given that this process is performed at lower temperatures, the heat losses caused by the high thermal diffusivity of copper are reduced [K02];
4. FSW welded joints have a finer microstructure and therefore improved mechanical properties [A05, B05, J05, S05];
5. It can be made in horizontal, vertical or circular direction, both in end-to-end positions and in overlapping positions, because it does not have a bath of molten material [A05, D04, O02];
6. It is a simple welding process, without consumables or additives [D04];
7. It is presented as "green technology" due to its energy efficiency and environmental protection [A04, A05, G04, N05, O02];
8. Does not require special preparation of parts before carrying out the process [J05, O02];
9. It does not depend on the skills of the operator [A04, M12, O02, S05];
10. It is an easy to automate process, with good repeatability [B05].

The FSW process also has some disadvantages, such as:

1. The welding machine is massive and expensive;
2. Has low welding speeds and high wear of the active element when joining materials with high melting temperature [C03];
3. The pin of the active element leaves a mark at the end of the welding bead;
4. Joints require good orientation and fixing [D04, F01, J05];
5. Narrow or small elements cannot be joined [O02].

1.4. Types of friction stir welding processes

Due to the proven efficiency and innovative nature of this welding technique, several researches have been initiated which are oriented in two directions:

- on the study of classical FSW processes, both of parts made of the same material and of parts made of different materials, in different variants of their positioning;

- on the study of hybrid FSW processes (HFSW), in which an association of the FSW process with other welding processes is made, the FSW process being the dominant process.

Classic friction stir welding processes

According to the kinematics used during the process, two types of processes are distinguished:

- *linear welding* (**FSW** - Friction Stir Welding);

- *spot welding* (**FSSW** - Friction Stir Spot Welding).

Linear FSW welding consists, as previously presented, in the non-removable assembly of two parts, by making a linear welding bead (Fig. 1.2.1).

FSW spot welding (FSSW) is a process similar to rotary active element friction welding (FSW), except that the active element no longer performs the forward movement in the direction of the weld bead.

Hybrid friction stir welding processes

The hybrid friction stir welding process, HFSW, has combinations between the FSW process and another melt welding process, in which the FSW process is the dominant process and the other process is used to generate an additional amount of heat at the level of welding parts. HFSW processes are mainly developed for joining high melting point materials, including copper, steels, stainless steels, nickel and titanium [B13, C03], as well as joining different materials, by raising the temperature of the higher melting point material. , in order to equalize their plasticities [Y01].

It is noted that for high melting point materials, bonded by FSW, such as steel, titanium and molybdenum, problems are identified in terms of high stress on the active element and the technological system, which lead to wear and damage of the rigidity of these elements [F04].

From the studied literature, it results that several types of HFSW processes have been analyzed and developed, in which the additional thermal input is generated by the following welding techniques:

- with laser beam, LAFSW (Laser Assisted Friction Stir Welding),

- with tungsten electrode in inert gas, FSW-TIG (Tungsten Inert Gas assisted Friction Stir Welding),

- with plasma arc, P-FSW (Plasma assisted Friction Stir Welding),

- by electric resistance, EAFSW (Electrically Assisted Friction Stir Welding).

For example, the working principle of the FSW-TIG process is similar to that of the FSW process, the only difference being that the rotating active element is preceded in the welding direction by the TIG torch (Fig. 1.4.6).

Sinclair and co-workers reported that the additional heat input from the TIG source leads to a significant 43 % reduction in axial force for a wide range of welding parameters. An increase in the flow of material in the weld bead was also observed, resulting in a wider welded joint, which defines stronger welds [S13].

Bang and co-workers [B03] also used the TIG assisted FSW process to bond Al with a Ti alloy. They reported that elongation and joint strength increase significantly compared to classic FSW welds. This technique has been used both to extend the life of the active element and to improve the efficiency of joining metallic materials with high melting temperature.

In addition to the technological parameters specific to the FSW process, the application of the additional heat input generated by the TIG source involves the adjustment of the following parameters [S11]: distance [mm] between the TIG electric arc and the rotating active element, TIG source intensity, I [A], and voltage, U [V].

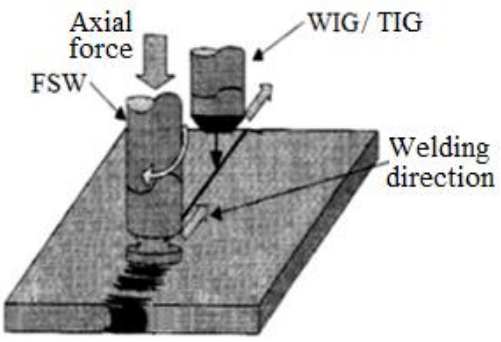

Fig. 1.4.6. Schematic representation of the TIG assisted FSW process [D05]

1.5. Material types welded by friction stir welding process

Given that the FSW process was developed for use in the welding of parts of aluminum alloys, it is easy to understand why, to date, most papers published worldwide refer to the joining of these alloys, whether we refer to when joining materials of the same type (Fig. 1.5.1), or when joining different materials (Fig. 1.5.2).

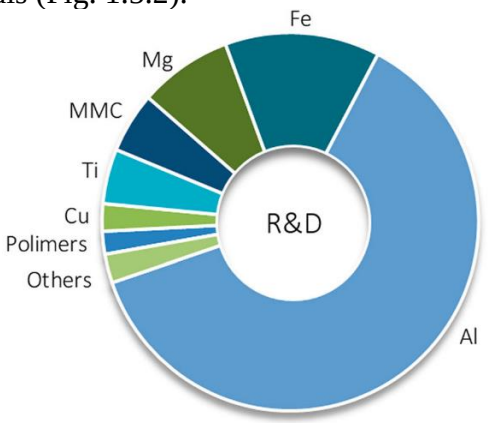

Fig. 1.5.1. Similar materials welded by FSW [M01]

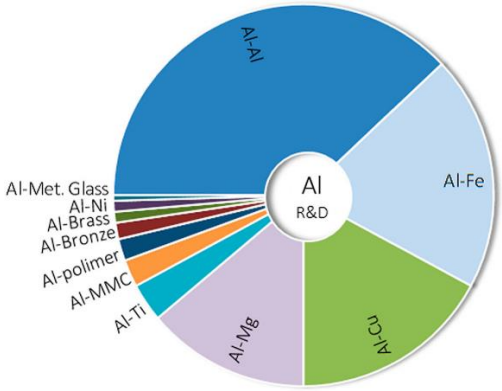

Fig. 1.5.2. Different materials welded by FSW [M01]

1.6. The rotating active element

The rotating active element (Fig. 1.6.1) is relatively simple from a constructive point of view and fulfills three main functions in the FSW welding process [Z08]: it heats the welding parts, by friction and plastic deformation, mixes the materials to form the cord welding and concentrates the flow of material under the shoulder and around the pin.

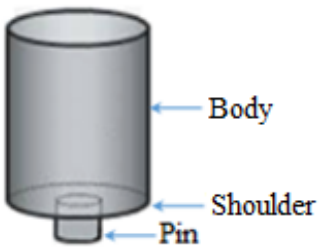

Fig. 1.6.1. Schematic presentation of the active element

Fig. 1.6.3. Types of channels on the active surface of the active element shoulder [G02]

In defining the geometry of the active element, the sizing of the two most important parts of it (shoulder and pin) is of main interest.

The shoulder of the active element has the role of ensuring the thermal input necessary to achieve the joint that is due to its friction with the surface of the joints [D01] and to retain the mixed pine material below it, thus ensuring the compactness of the joint [B01]. Thus, its constructive shape can be flat, concave or convex, and on the active surface of the shoulder can be processed various types of channels, striations, grooves, which have the role of increasing the ability of the shoulder to deform the materials of the joints, directing then to the pin (Fig. 1.6.3) [M06].

The pin of the active element has the role to ensure the thermal input necessary to achieve the joint, which is due to the plastic deformations made by it, and to mix and transfer the material of the parts to be welded in front of the active element behind it. In general, two outer shapes of the active element pin are used, cylindrical (Fig. 1.6.1) and conical (Fig. 1.6.3), on which various grooves, threads and flattenings can also be processed [Z03].

In FSW welding of copper, the concave or flat shoulder was generally used in combination with a cylindrical or conical pin, smooth or threaded. The pin length of the active element was generally reported to be 0.2 mm less than the thickness of the parts to be welded. The diameter of the pin is chosen, in most cases, slightly larger than the thickness of the parts to be welded [G04], while the diameter of the shoulder is 3 - 4 times larger than it.

The material of the active element must withstand the mechanical and thermal stresses that occur during FSW welding, having the following basic characteristics: mechanical resistance to ambient and high temperatures, chemical stability at high temperatures, lack of reactivity to welded materials, strength at wear, low coefficient of thermal expansion and good workability. A division of the most well-known materials used for the construction of the active element according to the material of the parts to be welded, is presented in the extended version of this work.

The geometries and materials of the active elements used in the HFSW processes are identical to those used in the FSW process [C12, M05, S11, Y01].

1.7. Friction stir welding equipment

FSW welding machines can be milling machines, special FSW welding machines or multi-articulated robots for FSW welding, each with its advantages and disadvantages.

1.8. Industrial applications of friction stir welding process

The main industrial fields in which FSW welding processes are used are transport, metalworking, research and development and electronics [M01].

Numerous potential applications of these technologies have been identified for the combination of copper and copper based alloys, but few have been evaluated [M11]. Research available in the field of FSW has focused on the manufacture of oxygen free copper (Cu-OF) containers for nuclear waste retention, the manufacture of copper support plates used in spray deposition processes and other restricted applications, in which research The FSW connection of copper alloys has so far been poorly documented [N01, O01].

Related research topics with significant applicability potential refer to the combination of different materials such as Al alloys with Cu alloys [N01].

Chapter 2. Characteristics of friction stir welded copper structures with rotating active element without or with additional heat input

Scientific research on welded joints by FSW and HFSW processes aims, where appropriate, to analyze one or more characteristics of these types of joints, the interdependence between them or their dependence on the type of welded materials, the type of process used or technological parameters. Given the topic addressed in this paper, the following subchapters will mainly present characteristics of the FSW and HFSW joints of copper and its alloys.

2.1. Technological parameters and temperature within the process

The rotational speed of the active element is the most important technological parameter of the FSW process, given that it is directly responsible for generating the temperature needed to carry out the process and for controlling, mixing, homogenizing and transferring the joined materials in front of the pin behind it [S05]. The recommended range for the active element rotational speed, at the FSW copper joint, is between 800 - 1200 rpm [M13].

The welding speed of the active element also has important implications in generating the temperatures necessary to carry out the process and in mixing, homogenizing and transferring the combined materials, because this parameter determines the duration of maintenance of the active element involved in rotational motion on a certain joint length. In general, the welding speeds identified in the literature were between 25 and 250 mm/min [S12, S17].

The application of axial force aims to keep the shoulder of the active element in contact with the surface of the joints to ensure the heat input due to friction [M12] and to retain the mixed material under the shoulder of the active element, thus ensuring the compactness of the joint [B01].

Tool tilt angle helps to obtain a higher pressing force. For the FSW joint of copper, the angle of inclination of the active element is 1 - 3º [H07, X01].

The most important technological parameter specific to HFSW processes is represented by the intensity of the additional heat input, which must be adjusted so that the temperature reached during the process does not exceed 70 - 80 % of the melting temperature of the material to be welded [S11].

Another technological parameter specific to HFSW processes is the distance between the point of application of the additional heat source and the rotating active element. Values indicating the positioning of the additional heat source in the immediate vicinity of the active element (13 mm [Y01], 25 mm [M05], 40 mm [C02], 43 - 44 mm [C12]) were used for this parameter.

The recommendations identified in the literature regarding the temperature required to make a FSW copper joint are different; In some works, it has been estimated that the maximum temperatures recorded in the process must be in the range of **(0.7 - 0.95) * T_{top}** [M12, P03, S05]. In other works, it is mentioned that, in order to obtain good mechanical properties when joining copper using the FSW process, it is recommended that the temperature recorded during the process be in the range of **(0.4 - 0.5) * T_{top}** [H07].

2.2. Visual aspect of friction stir welded joints

The visual aspect of the FSW and HFSW welding beads shows a succession of circular marks specific to these types of joints, which are due to the contact between the shoulder of the active element and the material to be welded (Fig. 2.2.1). Also, on the face of the joint, at the end of the welding bead, at the point where the retraction stage of the active element takes place, its pin leaves a hole of similar dimensions to its dimensions (Fig. 2.2.1).

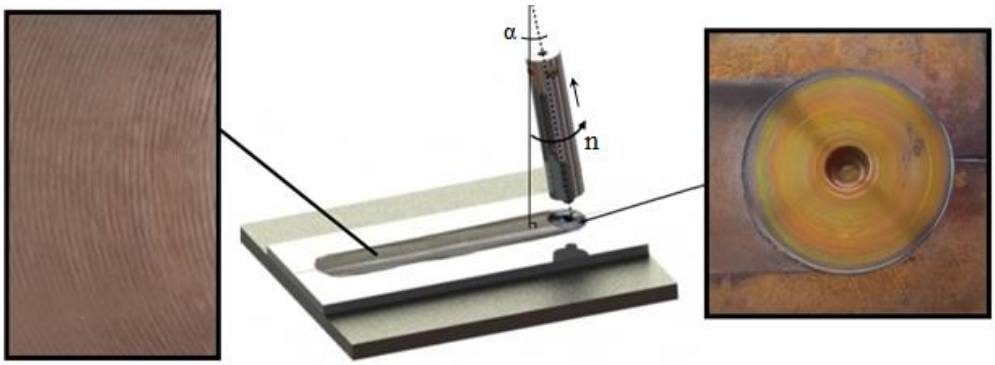

Fig. 2.2.1. Aspect of FSW and HFSW copper joints [adapted from L02]

2.3. Macrostructure of friction stir welded joints

FSW joints are characterized by a heterogeneous macrostructure of the weld bead. Studies of the FSW process unanimously present the number and name of the macroscopic areas that form the FSW joint (Fig. 2.3.1 - 2.3.2). Based on the microstructural characterization of grain size and orientation and precipitation, properties of these areas have been identified [J06, L04, M08]:

The core (NZ - Nugget Zone) is the area in the center of the joint, which records the highest temperature and the most severe plastic deformation during the process, phenomena that determine the dynamic recrystallization of this area.

The Thermo-Mechanically Affected Zone (TMAZ) is the area surrounding the core. In TMAZ, the deformations and temperatures recorded are lower than those recorded in the welding core, resulting in only a partial recrystallization.

The Heat Affected Zone (HAZ) is the area surrounding TMAZ, in which the recorded plastic deformation is not noticeable, but which still shows changes in the properties of the welded material due to the temperatures to which it is subjected during the process.

The Base Material (BM) is the part of the assembly that has not been subjected to any mechanical deformation. The heating of this area is not important, and the material retains its initial microstructure and mechanical properties.

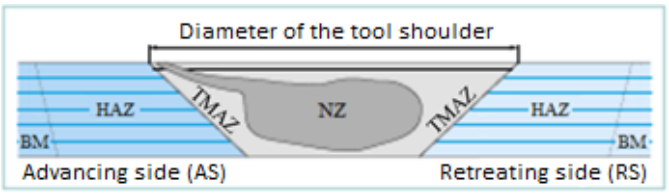

Fig. 2.3.1. Macrostructural areas specific to FSW joints [J06, M08]

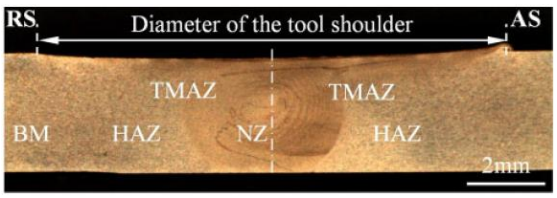

Fig. 2.3.2. Typical macrostructure of a FSW copper joint [L04]

Knowing that HFSW processes are derived from the FSW process, the macroscopic aspect of these joints is similar to that of FSW joints [L02].

2.4. Microstructure of friction stir welded joints

The microstructural aspect of the core of some FSW joints made at different rotational speeds of the active element is presented in Fig. 2.4.1.a-c. The grain size is predominantly determined by two factors, the degree of deformation and the temperature recorded during the process [L04, M13]. Increasing the degree of deformation during FSW joining causes a reduction in the size of the recrystallized grains, according to the general principle of recrystallization [H06]. Meanwhile, the increase in the maximum temperature recorded in the FSW process leads to a remarkable increase in grains.

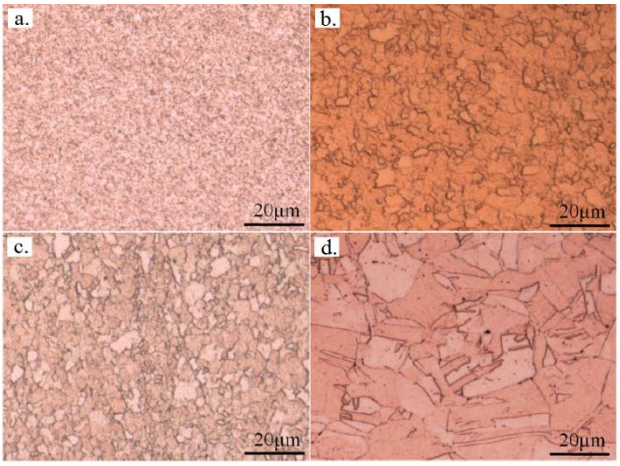

Fig. 2.4.1. Core microstructure made at a rotational speed of: (a) 300 rpm, (b) 600 rpm, (c) 800 rpm, (d) BM [L04]

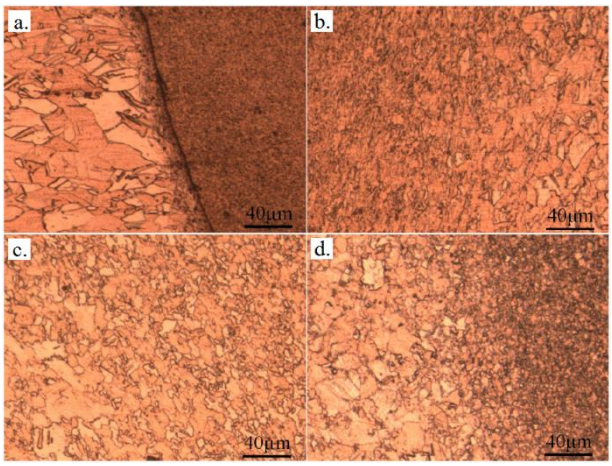

Fig. 2.4.2. TMAZ microstructure made at a rotational speed of: (a) 300 rpm on AS, (b) 300 rpm on RS, (c) 600 rpm on AS, (d) 800 rpm on AS [L04]

The TMAZ microstructure of the same joints is shown in Fig. 2.4.2. When the rotational speed of the active element is low, the TMAZ is quite narrow and there is a well-defined boundary between the TMAZ and the core (Fig. 2.4.2.a). As the rotational speed of the active element increases, the TMAZ becomes wider and the boundary between these two areas disappears, and the size of the grains in the TMAZ increases (Fig. 2.4.2.c-d). HAZ grains are somewhat larger than the base material grains.

With the transition from the FSW process to the HFSW process, it was observed that the grain size increases due to the application of additional heat input [L04, M13].

2.5. Microhardness of friction stir welded joints

The microhardness of FSW joints in copper alloys is influenced by two competitive mechanisms: softening annealing and grains refinement [S05]. In FSW welding the thermal input increases with increasing rotational speed of the active element and/or reducing the welding speed. This increase leads to softening annealing and thus to a lower hardness. The decrease of the registered thermal input leads to a finer granulation and, consequently, to a weld hardness equal to or even higher than that of the base material, Fig. 2.5.1 [S06, X01].

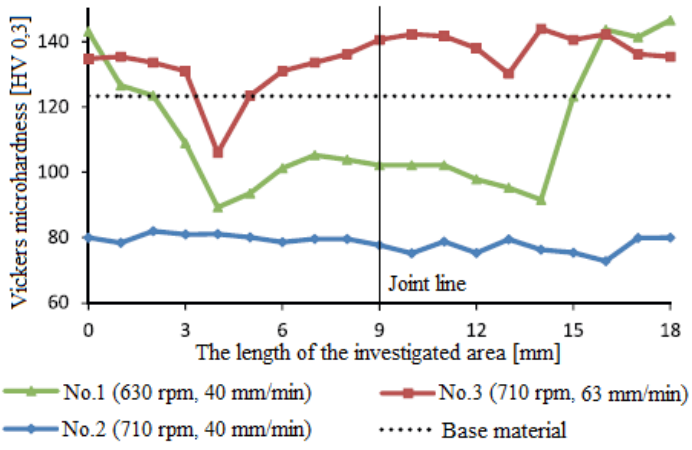

Fig. 2.5.1. Microhardness evolution of FSW copper joints in transverse direction [P03]

As mentioned earlier, with the transition from the FSW process to the HFSW process, the grain size increases due to the increase in temperatures recorded in the process, and this increase in grain leads to a decrease in the hardness of the made welds [M13].

2.6. Tensile strength of friction stir welded joints

The FSW joints of copper alloys have tensile strengths comparable to those of base materials. The tensile strength of pure copper FSW joints is slightly lower than that of the base material, reaching values of up to about 87 % of its mechanical strength [A06, L01], but slightly higher than that of EBW joints [O01].

The tensile strength and specific elongation of some FSW joints of pure copper made at different rotational speeds of the active element, with a constant welding speed of 100 mm/min are shown in Fig. 2.6.1. It can be seen that the tensile strength and the specific elongation have the same tendencies of variation. When the rotational speed of the active element varies in a range of low values, both the tensile strength and the specific elongation increase as the rotational speed of the active element increases and when the rotational speed increases over this range, both the tensile strength and specific elongation decrease.

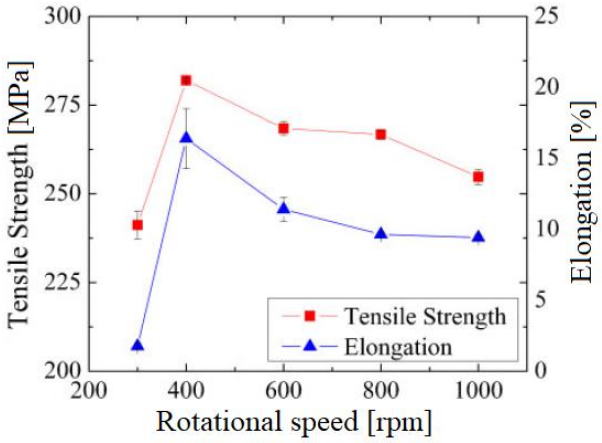

Fig. 2.6.1. Variation of tensile properties depending on the rotational speed of the active element [L04]

In the case of aluminum alloys, the transition from the FSW process to the HFSW process does not produce significant changes on the mechanical strength of the joints made [C03]. In contrast, in the case of copper alloys, it has been reported that as heat input increases, grain size increases and mechanical strength of joints decreases [M13].

2.7. Defects of friction stir welded joints

Defects encountered in FSW welds can be of two types: aspect or visible defects and defects inside the weld beads. Savolainen [S05] made a schematic representation of the aspect and location of welding defects of FSW copper joints (Fig. 2.7.1).

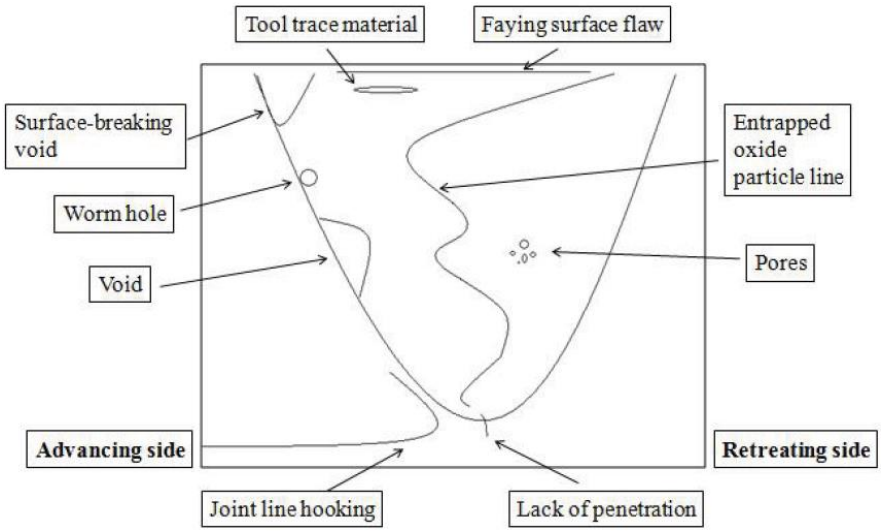

Fig. 2.7.1. Schematic representation of the location of the FSW copper joints defects [S05]

Chapter 3. Research on numerical modeling and simulation of friction stir welding process with rotating active element without or with additional heat input

3.1. Development of the numerical model of friction stir welding process with rotating active element

Due to the demonstrated efficiency and innovative nature of the FSW process, several actions have been initiated to optimize it. One of these actions is the numerical modeling and simulation of this process. Numerical simulation helps to better understand and observe the influence of input parameters on the phenomena in the process and the made joints.

Due to the important deformations registered in the process and the modification of the properties of the welding materials depending on the temperature, the development of a valid numerical simulation is a difficult task. For this reason, several methods for the numerical simulation of this procedure have been approached in the literature, the most important of which are: Lagrange method, Euler method, ALE method (Arbitrary Lagrangian-Eulerian) and CEL method (Coupled Eulerian-Lagrangian).

Regardless of the method used, for the development of such a numerical model, the following activities must be performed: defining the geometry of the constituent elements and their assembly, defining the material properties and constitutive equations, defining the type of contact between surfaces, establishing the boundary conditions, meshing the constituent elements; validation of the numerical model. Thus, these activities will be briefly presented in the following sections.

Defining the geometry of the constituent elements and their assembly

The definition of the geometry of the constituent elements is generally made starting from the shape and dimensions of the elements used experimentally, by correspondingly defining them according to the method used and the results followed in the simulation (Fig. 3.2.1).

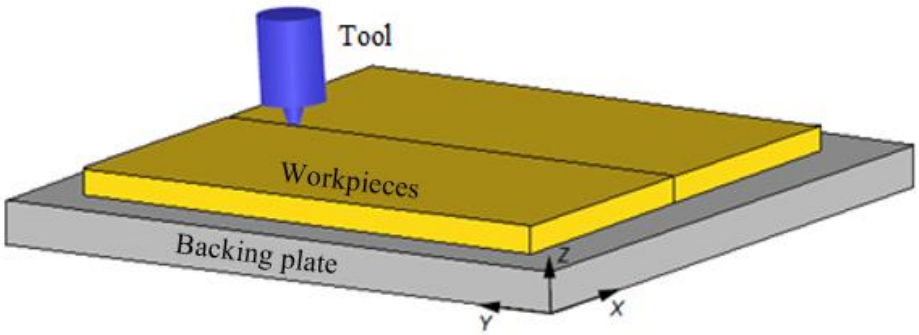

Fig. 3.2.1. The set of constituent elements of an FSW/ HFSW joint [J04]

Defining material properties and constitutive equations

During the FSW process, the material to be welded is subjected to wide variations of temperatures and deformations, which lead to changes in its behavior. Thus, for the development of a numerical model it is necessary to use a constitutive equation that defines the behavior of the material throughout the process. Several constitutive equations have been reported in the literature, including Johnson-Cook, Sheppard-Wright and Norton-Hoff. Of these, the most commonly used constitutive equation is Johnson-Cook, which defines the plastic behavior of the materials to be welded based on the relationship between the flow stress σ, the strain rate ε and the recorded temperature T.

Defining the type of contact between surfaces

Interactions in the numerical model are defined to mimic physical phenomena. They are defined between different constituent elements to allow the transfer of heat and forces between them. Thus, there can be two types of interactions: mechanical and thermal.

Mechanical interactions. The 'Penalty contact' contact algorithm is the most commonly used algorithm for nonlinear contact conditions. Several laws were used to determine the tangential stress on the contact surface between the active element and the parts to be welded, such as: Coulomb's law [A03, A10, L03], modified Coulomb's law [G07, L03, Z04], Norton's law [A10, L08] and the shear friction law [A09, B15, J03]. Because the best results were obtained with Coulomb's law, it is the most used.

Thermal interactions. In FSW, friction and plastic deformation contribute to the generation of heat needed to carry out the process. A certain percentage of the total heat generated is transferred to the active element and the base plate by conduction and to the environment by convection and radiation (Fig. 3.2.2). The amount left inside the welds raises their temperature [J04].

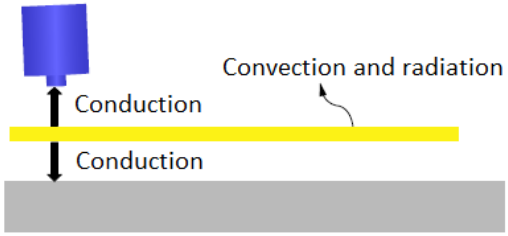

Fig. 3.2.2. Physical heat transfer between elements and the environment [J04]

The heating due to friction is incorporated in the calculation of the tangential frictional force defined on the contact surface (discussed in the previous section). The heating due to plastic deformation depends on the level of deformation and is directly related to the law of behavior of the materials to be welded [L08].

The amount of heat transferred from the parts to the active element (Q_{wt}), the amount transferred from the parts to the baseplate (Q_{wb}) and that transferred from the parts to the environment (Q_{wa}) are calculated in the structure of numerical models by means of transfer coefficients convective heat transfer, which are defined so that the resulting convective heat transfer between these elements is equivalent to the convective/ conductive heat transfer physically performed between them (Fig. 3.2.2).

Establishing the boundary conditions

The parts to be welded can be constrained in various variants to reproduce the experimental conditions. One of the variants is the embedding of the side faces, in order to eliminate any movement of them. Rotational and translational movements are imposed on the active element depending on each stage of the process. Therefore, it has a rotational movement around the Z axis and a translational movement on the Z axis for the penetration stage, or on the Y axis for the effective welding stage.

Mesh of the constituent elements

Meshing of a constituent element represents its division into a certain number of finite elements, in order to further analyze each element [J04]. In this stage of the development of numerical models are highlighted more clearly the specific characteristics of each method (Lagrange, Euler, ALE, CEL), characteristics that are presented in the extended version of this paper and largely related to the movement of mesh nodes and material points.

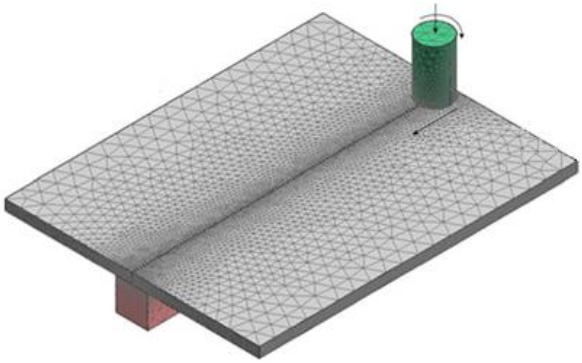

Fig. 3.2.5. Mesh of welding parts and active element [H01]

Regardless of the method chosen, the meshing of the parts to be welded in the area of the joint line is finer than in their other areas (Fig. 3.2.5), but the type of finite elements must be chosen in accordance with the numerical modeling method used.

Validation of the numerical model of friction stir welding process (FSW)

In order to validate the numerical model, the values recorded in the numerical simulation are compared with those determined experimentally, for different characteristics of the welded joints. Thus, model validation is performed using at least one of the following methods:

- analysis of the temperature distribution in the welding bead, but also its evolution in time [A10, B08, D03, G05, G06, J02, L03, L08, M04, P05, S01, Z07],
- analysis of the axial force [A10, K02, M04] and the torque at which the active element is subjected [T04],
- analysis of the residual stress distribution [A11, G06],
- analysis of microhardnesses measured in different areas [P02].

3.2. Development of the numerical model of friction stir welding process with rotating active element and additional heat input

In the identified works it is reported that the numerical modeling of the HFSW process is performed starting from the validated numerical model of the FSW process, which is subsequently modified to include the additional heat input, characteristic of HFSW processes [D02]. Thus, in order to achieve a valid numerical model of the HFSW process, the activities mentioned above must be performed, which are specific to the development of the numerical model of the FSW process, to which is added this new activity represented by modeling the additional heat input.

Thus, to perform numerical modeling of the HFSW process, the validated numerical model of the FSW process is modified to include the additional heat input [D02, S11, Y01]. For example, the additional heat input due to a laser source is modeled as a circular heat flux on the upper surface of the parts to be welded, before the active element, which is calculated using the Gaussian equation. This heat flux is defined over a specific area and varies according to spatial and time coordinates, similar to the heat flux generated in the FSW process.

3.3. Results of the numerical simulation of friction stir welding process with rotating active element and additional heat input

Daftardar [D02] developed, in the Fluent software, a numerical model for the laser assisted FSW joining of an aluminum alloy. It was based on a validated numerical model of the FSW process, which was also assigned the additional heat input generated by the laser beam. To compare the FSW process with the HFSW process, the maximum temperature recorded within them, at an arbitrarily chosen point, was kept constant for both processes at a value of 400 °C. To achieve this, changes were made to the technological parameters of the HFSW process, so that the heat generated by the active element is reduced. From this comparative analysis it is observed that the temperature in front of the active element in the FSW process, after 60 seconds, is 183 °C, and in the HFSW process it is 345 °C (Fig. 3.3.1). This means that mixing in the HFSW takes place in a softer area than in the conventional FSW, due to the additional heat input (lower wear, higher welding speeds).

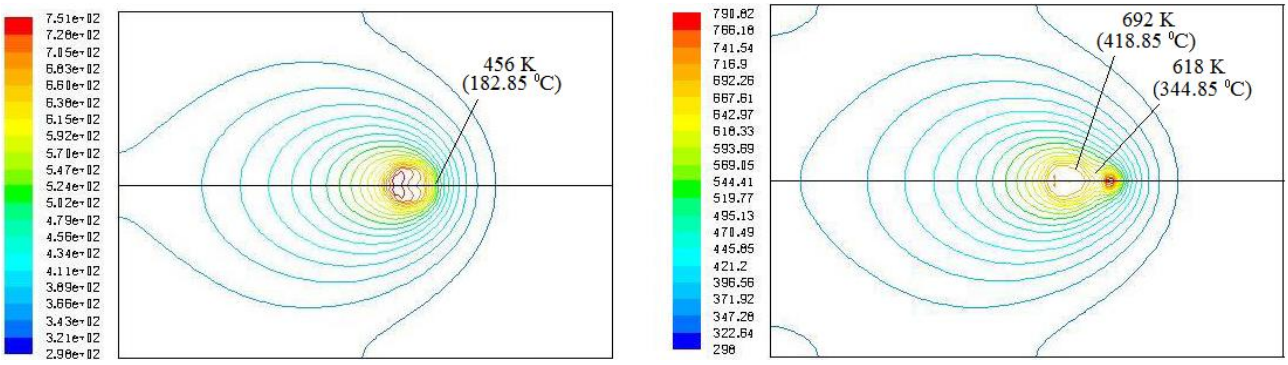

Fig. 3.3.1. Outlines of temperatures resulting from
FSW and HFSW (laser assisted) processes after 60 s [D02]

Scutelnicu and his collaborators [S11] developed, in the MSC Marc software, a finite element numerical model, which simulates TIG assisted FSW welding of copper, in order to predict the temperature distribution and the maximum temperature recorded during the process. This model was also based on a validated numerical model of the FSW process, both numerical models being validated using the infrared thermography method. The results obtained from these numerical simulations being similar to those reported by Daftardar [D02].

Chapter 4. Conclusions on the current state of research and development of friction stir welding processes and systems with rotating active element without or with additional heat input

From the analysis of the current state of research-development of the friction welding process with rotating active element and additional heat input, important conclusions can be drawn, as follows.

• Copper and copper based alloys offer unique combinations of electrical and thermal conductivity, mechanical strength, formability and corrosion resistance and are used in a wide range of engineering applications (see § 1.1).

• Joining elements of copper or copper based alloys is usually done by various melting welding processes, soldering joining processes and solid state welding processes. However, the weldability of copper and its alloys by fusion welding processes is affected by certain factors. Soldering and solid-state welding processes avoid these problems associated with melting welding processes, but of these only solid-state welding processes can achieve joints with mechanical strength similar to melting joints (see § 1.1).

• Friction stir welding (FSW) is a solid-state joining process that is based on the heat generated by the friction and plastic deformation made by a non-consumable welding tool, called active element, when interacting with the parts to be joined. It is performed in four stages: the penetration stage, the maintenance stage, the effective welding stage and the withdrawal stage. The process parameters characteristic of this process are related to the positioning of the active element during the welding process and to the movements it performs: inclination angle, rotational speed, welding speed, axial process force (see § 1.2).

• Due to its solid nature, the FSW process has many advantages compared to conventional melt welding processes, such as: the ability to weld alloys of materials that are largely non-weldable or difficult to weld using melt welding processes, the ability to weld different materials, generating finer microstructures and therefore improved mechanical properties and eliminating the disadvantages associated with fusion welding processes (no additive material, shielding gas, oxide removal, allows welding in any position and reduces losses high heat recorded when welding materials with high thermal diffusivity) (see § 1.3).

• The FSW process also has some disadvantages, such as: the welding machine is massive and expensive, has low welding speeds and high wear of the active element when joining materials with high melting temperature, the pin of the active element leaves a mark at the end of the welding bead and narrow or small parts cannot be joined (see § 1.3).

• Due to the demonstrated efficiency and innovative nature of this welding technique, several researches have been initiated in two directions: on the study of classical FSW welding processes and on the study of hybrid FSW welding processes (HFSW). HFSW processes have combinations between the FSW process and another melt welding process, in which the FSW process is the dominant process and the other process is used for the local application of an additional amount of heat to the parts to be welded, just before the FSW welding area (see § 1.4).

• The most commonly joined materials using the FSW process are aluminum alloys, followed by iron, magnesium, metal matrix composites, titanium and copper alloys. The most common combinations of different materials that have been combined using the FSW process are Al-Al combinations, followed by Al-Fe, Al-Cu and Al-Mg combinations. HFSW processes are mainly used for joining materials with high melting temperatures and for joining different materials, where the classical FSW process has some limitations (see § 1.5).

• The rotating active element is relatively simple from a constructive point of view and fulfills three main functions in the FSW welding process: it produces the heating of the welding parts by friction and plastic deformation, mixes their materials to form the welding bead and concentrates the material flow around the pin and under his shoulder. The geometry and dimensions of the shoulder and pin of the active element vary depending on the thickness and material of the parts to be welded and considerably influence the quality of the joints made. Its material must have the following basic characteristics: mechanical strength and chemical stability at high temperatures, lack of reactivity to welded materials, wear resistance, low coefficient of thermal expansion and good workability. The geometries and materials of the active elements used in the HFSW processes are identical to those used in the FSW process (see § 1.6).

• FSW welding equipment is classified into three categories, each with its own advantages and disadvantages, respectively: milling machines, special machines for FSW welding and polyarticular robots for FSW welding (see § 1.7).

• FSW welding processes are used in various industries for the manufacture of components, especially aluminum alloys. Numerous applications are identified for the combination of copper and copper based alloys, but few of them have been made. Thus, research has focused on the manufacture of oxygen free copper containers for nuclear waste retention, copper support plates used in spray deposition processes, copper water cooled supports and other restricted applications (see § 1.8).

• The recommended range for the rotational speed of the active element, at the FSW joint of the copper, is 800 - 1200 rpm, and for the welding speed of 25 - 250 mm/min. The axial force aims to keep the shoulder of the active element in contact with the upper surface of the parts to be joined. Increasing the rotational speed of the active element, the axial force applied to it or decreasing its welding speed causes an increase in the temperatures recorded in the process (see § 2.1).

• The thermal input required to make a FSW joint of copper is much higher than that required to make an FSW joint of another material, due to the high thermal diffusivity of copper alloys and especially pure copper. This drawback can be overcome by performing FSW joints at lower welding speeds and/or higher rotational speeds. Therefore, the FSW bonding of copper alloys is limited to a limited range of technological parameters, due to the relatively high melting temperature and the high thermal diffusivity of these materials. Thus, the introduction of an additional heat source in the process is beneficial in terms of increasing the welding speed and, implicitly, the productivity of the process. This makes the use of HFSW processes suitable for this category of materials (see § 2.1).

• The recommendations identified in the literature regarding the temperature required to achieve a FSW copper joint are different. While in some works it is recommended that the temperatures generated during the process be 0.7 - 0.95 of the melting temperature of the base material, in other works it is recommended that they be 0.4 - 0.5 from the melting temperature of the base material (see § 2.1).

• The visual aspect of the FSW and HFSW welding beads showed a succession of circular marks due to the contact between the shoulder of the active element and the material of the parts to be welded and at their end a hole similar in size to the pin of the active element, left by it when withdrawing from the material of the parts to be welded (see § 2.2).

• FSW and HFSW processes generate important changes in the macrostructural and microstructural characteristics of the materials to be welded, both in the area of the weld bead and in the adjacent areas, leading to the establishment of four macrostructural areas specific to these types of joints: joint core (NZ), thermo-mechanically affected zone (TMAZ), heat affected zone (HAZ), base material (BM) (see § 2.3).

• The core of FSW copper joints has small equiaxial grains. TMAZ is not as clearly distinguished as in the case of FSW aluminum joints, because it does not have elongated or rotated grains in the area adjacent to the core, so under certain conditions its existence is difficult to highlight. HAZ has the same grain structure as the base material. Heat input and the degree of deformation play an important role in determining the grain size, which may exceed the grain size of the base material if the temperatures generated during the process are too high (see § 2.4).

• Increasing the temperature leads to a softening annealing and thus to a lower hardness. The decrease of the thermal input leads to a finer granulation and, consequently, to a weld hardness equal to or even higher than that of the base material. With the transition from the FSW process to the HFSW process, the grain size increases due to the increase in heat input, and this increase leads to a decrease in the hardness of copper alloy joints (see § 2.5).

• The microscopic changes produced by the FSW process also generate changes in the local and global mechanical behavior of the weld bead. The values of the tensile strengths of the FSW and HFSW joints of copper show the same mode of variation as the values of the microhardnesses (see § 2.6).

• Defects found in FSW joints of copper alloys can be of two types: aspect defects and defects inside the weld beads. Research has shown that defects in FSW copper joints are mainly caused by improper choice of the active element and process parameters, which can lead to excessive or insufficient heat, mixing or pressing forces (see § 2.7).

• Due to the problematic characteristics of the FSW process, mainly represented by the important deformations registered in the process and by the changes of the properties of the welding materials as a function of temperature, the development of a valid numerical simulation represents a difficult task. Thus, in the literature were approached several methods for numerical simulation of this procedure, of which the most important are: Lagrange method, Euler method, ALE method and CEL method. Regardless of the method used, for the development of such a numerical model, the following activities must be performed: defining the geometry of the constituent elements and their assembly, defining the material properties and constitutive equations, defining the type of contact between surfaces, establishing the boundary conditions, meshing the constituent elements and validating the numerical model (see § 3.1).

• The definition of the geometry of the constituent elements is made starting from the shape and dimensions of the elements used experimentally (see § 3.1.1).

• During the FSW process the material to be welded is subjected to wide variations of temperatures and deformations, which lead to changes in its behavior. Thus, for the development of a numerical model it is necessary to use a constitutive equation (often Johnson-Cook) that defines the behavior of the material throughout the process (see § 3.1.2).

• Interactions in the numerical model are defined to mimic physical phenomena. They are defined between different constituent elements to allow the transfer of heat and forces between them. Thus, there can be two types of interactions: mechanical and thermal (see § 3.1.3).

• The parts to be welded are constrained to reproduce their fixation, while rotational and translational movements are imposed on the active element depending on each stage of the process (see § 3.1.4).

• Meshing of a constituent element represents its division into a certain number of distinct finite elements, in order to further analyze each element. At this stage of the development of numerical models, the specific characteristics of each method are highlighted more clearly. The Euler and Lagrange formulations are the two classical methods for defining motion in continuous mechanics, and the ALE and CEL formulations are combinations of the classical methods that are used to overcome their individual disadvantages (see § 3.1.5).

• The validation of the FSW numerical model is performed by comparing the values calculated by it with the values determined experimentally, for different characteristics of the welded joints (see § 3.1.6).

• In order to achieve a valid numerical model of the HFSW process, all activities specific to the development of a numerical model of the FSW process must be performed, plus the modeling of the additional heat input. The additional heat input is modeled as a circular heat flux, which is applied before the active element and which has a Gaussian distribution in the material of the parts to be welded (see § 3.2).

• The analysis of the results obtained with the numerical modeling of HFSW processes shows that the mixing of the material takes place in a softer area than in the conventional FSW, that the effort exerted on the active element is diminished and implicitly its degree of wear is reduced. These findings indicate the possibility of achieving higher productivity by using this process (see § 3.3).

Part II.

Contributions to the theoretical-experimental development and numerical modeling of friction stir welding processes and systems with rotating active element without or with additional heat input of some Cu-DHP structures

Chapter 5. Directions, main objective and research and development methodology of friction stir welding processes and systems with rotating active element without or with additional heat input of some Cu-DHP structures

5.1. Research and development directions

Based on the analysis of the current state, it is estimated that the following research and development directions regarding the friction stir welding processes and systems with rotating active element without or with additional heat input, FSW, respectively, HFSW are relevant:

• knowledge development of the phenomena that occur in friction stir welding processes and systems with rotating active element without or with additional heat input, and accordingly, the relations between the characteristics of welding processes, welding systems and welded structures;

• development of technological characteristics of FSW and HFSW processes, in order to extend the industrial use;

• development of numerical models for the simulation of FSW and HFSW welding processes, in order to reduce the costs of analysis and industrial implementation.

5.2. The main objective of the research and development activity

Considering the data and conclusions derived from the analysis of the current state, as well as the research-development directions regarding the HFSW welding process, it is determined as the main objective of the research-development activity within the doctorate: **development, through theoretical-experimental research and numerical modeling, of friction stir welding processes and systems with rotating active element without or with additional heat input of some copper structures.**

5.3. Research and development methodology

The research-development methodology is designed as a reference system for the actions that will be undertaken in order to fulfill the main objective of the advanced doctoral activity and consists in carrying out the following activities that define the content of the following chapters of this doctoral thesis:

(1) Carrying out preliminary theoretical-experimental research on the FSW process and the FSW-TIG process, in order to establish the influence that some technological parameters of these processes have on some process characteristics and on some characteristics of the resulting joints.

(2) Carrying out advanced theoretical-experimental research aimed at validating the most favorable technological conditions resulting from the preliminary theoretical-experimental research of the FSW process and extrapolating these conditions to the FSW-TIG hybrid process.

(3) Development, validation and operation of a thermomechanical coupled three-dimensional numerical model of the FSW process, for butt welding of two pure copper plates, and its extension for the FSW-TIG hybrid process.

Modeling of FSW and FSW-TIG processes in order to carry out theoretical-experimental research

The schematic representations of the two welding processes used in the research, that of the FSW process, respectively that of the FSW-TIG process, are presented in Fig. 5.3.1 - 5.3.2.

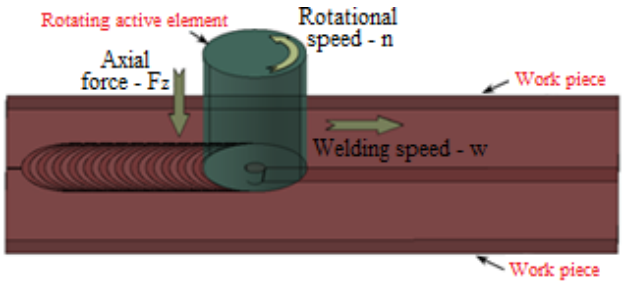

Fig. 5.3.1. Scheme of the FSW process

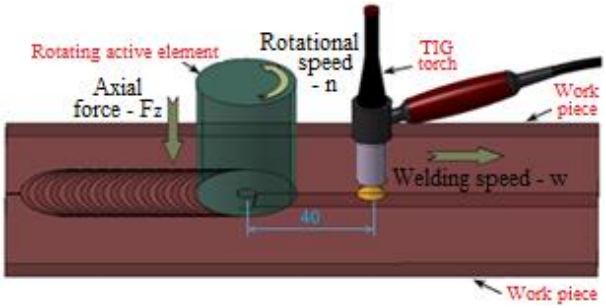

Fig. 5.3.2. Scheme of the FSW-TIG process

For research and development of FSW and FSW-TIG welding processes, analytical-empirical models will be used, starting from an input-output model of these processes (Fig. 5.3.3).

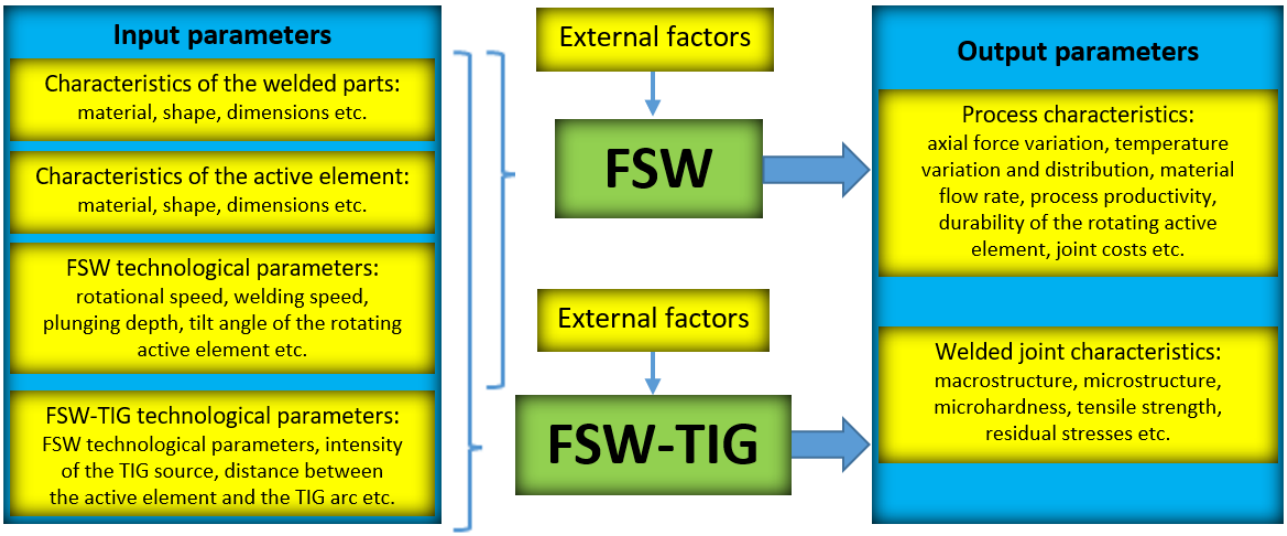

Fig. 5.3.3. FSW and FSW-TIG process modeling scheme

To limit the number of experiments, only the following technological parameters will be varied between the input parameters of the FSW and FSW-TIG processes, considered to have a significant influence on the process and characteristics of the welded joint, respectively:

FSW	- rotational speed of the active element, n, - welding speed, w,	FSW-TIG	- rotational speed of the active element, n, - welding speed, w, - the intensity of the TIG source, I.

FSW and FSW-TIG welding processes are characterized by:
- process temperature, T,
- axial process force, F_z.

Experiment planning

The experimental research of the FSW and FSW-TIG processes was performed on the basis of two experimental plans: a preliminary plan - based on the data identified in the literature and an advanced one - based on the data resulting from the preliminary one.

The preliminary experimental plan used for the FSW process analysis consists of a complete factorial plan with two levels, plus 2 more experiments (exp. 1.2 and 1.4) performed at the central value of the rotational speed, varying the welding speed, which are useful for the comparative

analysis of the two procedures (Fig. 5.3.4). The preliminary experimental plan used for the analysis of the FSW-TIG process consists of a complete factorial plan with two levels, with a single varied technological parameter: welding speed (Fig. 5.3.4).

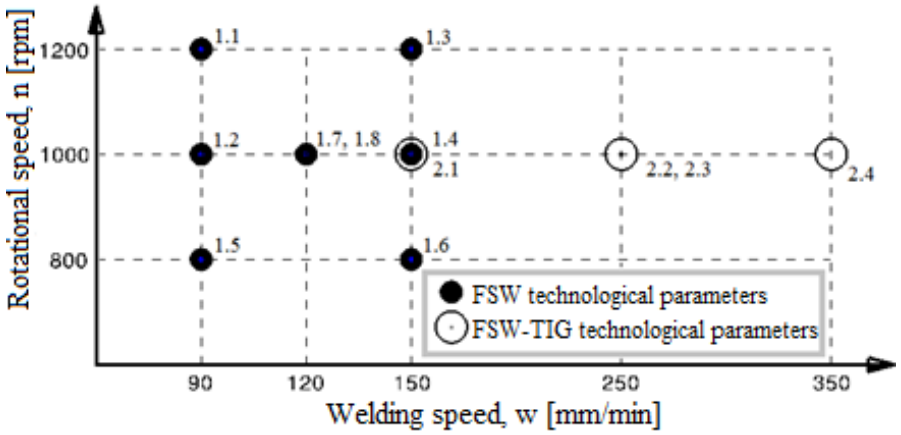

Fig. 5.3.4. Combinations of values of technological parameters in the preliminary experimental plans

The advanced experimental plans of the FSW and FSW-TIG processes (Table 5.3.4 - 5.3.5) are made after analyzing the characteristics of the preliminary joints, taking into account the identified dependencies. The justifications for choosing these new combinations of technological parameters are detailed in the chapter that presents the analysis of these joints' characteristics (see § 8.1).

Table 5.3.4. Advanced experimental plan of the FSW process

Exp. code	**Rotational speed, n** [rpm]	**Welding speed, w** [mm/min]
1.9	800	90
1.10	800	120
1.11	800	120
1.12	800	150

Table 5.3.5. Advanced experimental plan of the FSW-TIG process

Exp. code	**Rotational speed, n** [rpm]	**Welding speed, w** [mm/min]	**TIG source intensity, I** [A]
2.5	800	350	100
2.6	800	350	
2.7	800	250	
2.8	800	250	
2.9	1000	350	80
2.10	1000	250	

Planning the development of the numerical models

ABAQUS 6.13/ Explicit software will be used for the numerical simulation of the FSW-TIG process. The method used to make the numerical model is the CEL (Coupled Eulerian-Lagrangian) method. It was chosen because of its ability to handle large deformations and the ability to track the flow of material, which allows it to anticipate the formation of volume defects in welded joints.

Numerical modeling of the FSW-TIG process follows the research-development methodology by numerical modeling presented in the literature (see § 3.2).

Chapter 6. Elements of the experimental research system of friction stir welding processes with rotating active element without or with additional heat input of some Cu-DHP structures

6.1. The welded structure

The parts to be welded by the FSW and FSW-TIG processes are positioned end to end and have the shape and dimensions indicated in Fig. 6.1.1.

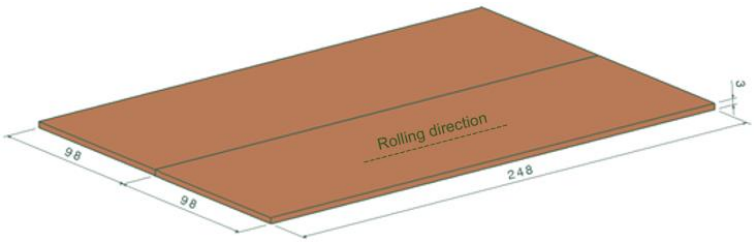

Fig. 6.1.1. Parts to be welded by FSW and FSW-TIG processes

The material from which the parts to be welded by FSW and FSW-TIG processes are made is Cu-DHP (phosphorus - deoxidized copper), a deoxidized copper alloy with a residual but limited amount of phosphorus (99,9 % copper and between 0,015 - 0,04 % phosphorus). Cu-DHP is used for the production of radiators, elements for air conditioners and refrigerators, tanks, heat exchangers etc.

To achieve the experiments, Cu-DHP sheets with dimensions of 2000 x 1000 x 3 mm, obtained by cold rolling, were purchased. All the parts to be welded were cut from these sheets of sheet metal with an automatic band saw, so that the side on which the joint is made is parallel to the rolling direction (Fig. 6.1.1).

6.2. Experimental stand and process characteristics measured in real time

The experimental stand consists of a specialized FSW welding machine, a TIG additional heating equipment, the rotating active element, a device for orienting and fixing the parts to be welded and various data acquisition, recording and monitoring systems (Fig. 6.2.1).

The experiments were performed on the FSW welding machine, type FSW-4-10, from ISIM Timisoara.

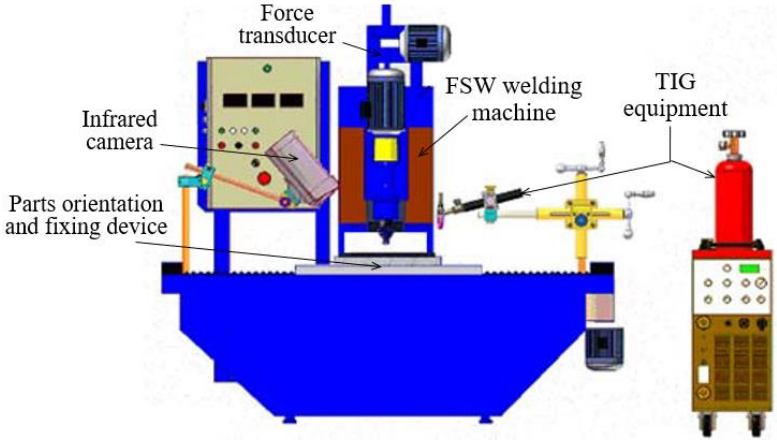

Fig. 6.2.1. Experimental stand [R03]

The TIG equipment used for the experiments is of the Kemppi MASTERTIG 2500 AC/ DC type and consists of: the heating unit, the protective gas cylinder, the torch and cables.

The orientation and fixing device of the parts (Fig. 6.2.4) was specially designed and made for these experiments, in order to ensure a precise and fast orientation of the parts to be joined.

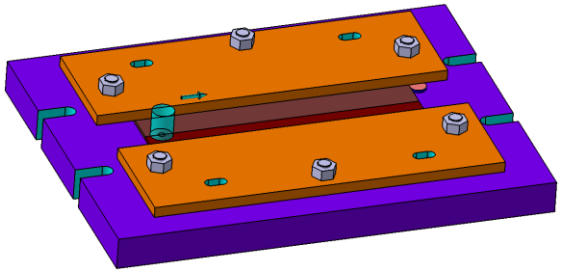

Fig. 6.2.4. The orientation and fixing device of the parts

The monitoring of the welding process is performed by recording and analyzing the values of temperature and axial force throughout the process. The process temperature was measured using the infrared thermography method, with an infrared thermographic camera type FLIR A40M. The axial process force was measured using a mechanical device mounted on the main shaft of the welding machine, which includes a sensor with a WIKA compression force transducer.

6.3. The rotating active element

The rotating active element used has a classic monoblock structure, with flat shoulder and smooth conical pin. Its shape and dimensions are shown in Fig. 6.3.1 and are in accordance with the recommendations identified in the literature (see § 1.6).

It is made of tool steel alloy, **P20+S** (40 CrMnMoS 86), pretreated, with a high resistance to mechanical stress and very good machinability properties by cutting.

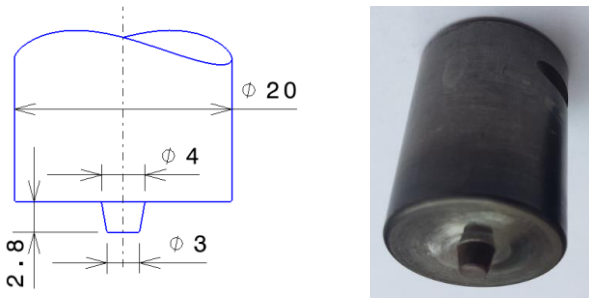

Fig. 6.3.1. Shape and dimensions of the rotating active element

6.4. Specimens sampling and coding

From the welded structures in the preliminary research were extracted three specimens for determining the roughness of the joints, two specimens for macrostructural, microstructural analysis and for determining the microhardness of the joints and three specimens for tensile testing (Fig. 6.4.1).

One specimen was extracted from the welded structures in the advanced research for the macrostructural, microstructural analysis and for determining the microhardness of the joints and three specimens for the tensile test and the roughness measurement. Compared to the preliminary research, the sampling of some specimens was abandoned, as a result of the conclusions drawn from the realization of the preliminary experiments and the analysis of the specific specimens (Fig. 6.4.2).

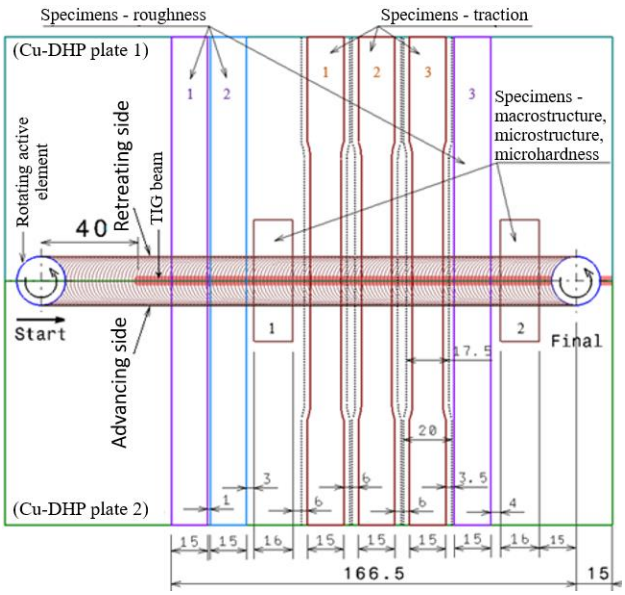

Fig. 6.4.1. Position of the specimens used to characterize welded structures in preliminary research

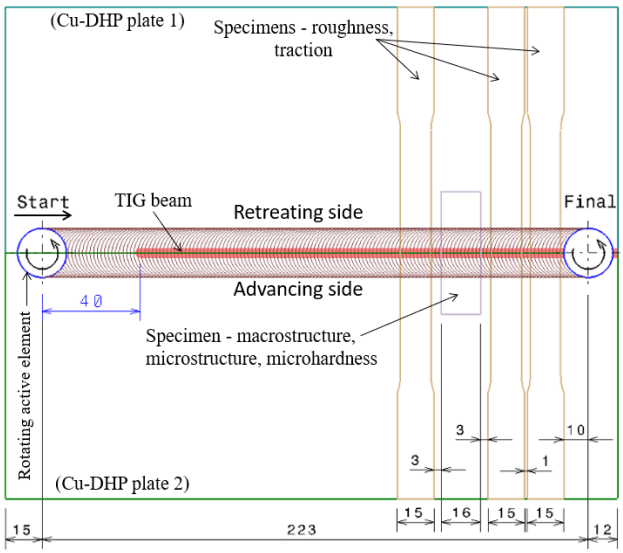

Fig. 6.4.2. Position of the specimens used to characterize welded structures in advanced research

All specimens were cut with a water jet. After sampling, the specimens were inscribed by mechanical engraving, according to the coding shown in Fig. 6.4.3.

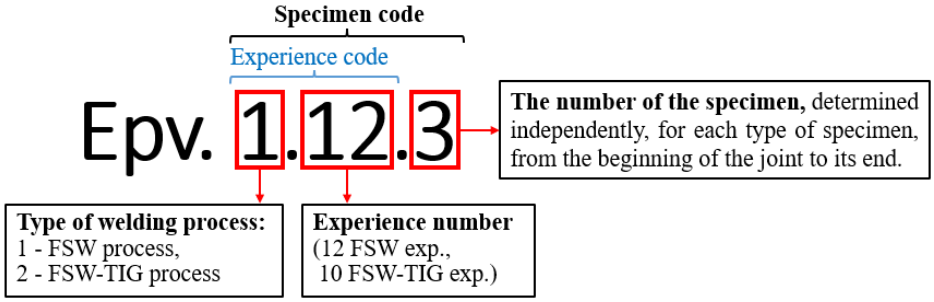

Fig. 6.4.3. Coding of the specimens sampled from welded structures

6.5. Specimens preparation

The specimens used to determine the tensile strength (Fig. 6.5.2) are of the *dumbbell* type and were made taking into account the dimensions recommended in the standard for tensile tests **SR EN ISO 6892-1**. Thus, the preparation of the specimens for the tensile test required the performance of additional machining by milling, after cutting with water jet, in order to ensure the dimensional characteristics required by this standard.

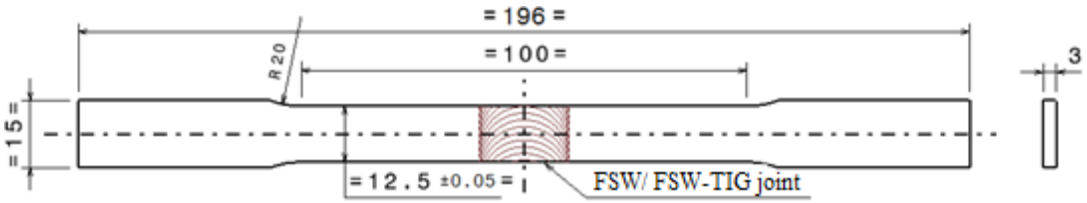

Fig. 6.5.2. Shape and dimensions of the specimens used to determine the tensile strength

In order to determine the local mechanical behavior of these joints (on each of their characteristic areas), which is briefly addressed in the literature (see § 2.6), for some of the specimens tested the Digital Image Correlation (DIC) method was also used. In principle, this method is based on the use of images recorded simultaneously by two video cameras, which, like the human eye, provide a spatial image of the analyzed object, thus allowing monitoring of displacement and deformation fields on different areas of the specimens during the tensile test.

The use of this method requires a random coding (of some freckles) on the analyzed areas of the specimens tested for traction (Fig. 6.5.3).

Fig. 6.5.3. Locating the investigated areas by correlating images

The specimens for the macrostructural, microstructural analysis and for the determination of the microhardness required additional sanding and polishing operations. The sanding of these specimens was done mechanically, with metallographic paper, under continuous water jet, so that the specimen does not heat above body temperature, using the two-plate sanding machine, Minitech 263. To improve the ergonomics and productivity of sanding these small specimens a device for orienting and fixing the specimens was made, with the help of which 2 or more specimens can be sanded simultaneously (Fig. 6.5.5).

Polishing was performed on the same machine as sanding, the metallographic paper being replaced with suede, and alumina (Al_2O_3) was used as polishing agent.

On the same specimens used in the macrostructural, microstructural analysis and in the determination of the microhardnesses, for which the mechanical sanding and polishing was performed, the chemical attack was performed, with a solution of nitric acid (HNO_3) in concentration of 65 %, to highlight the macrostructural and microstructural characteristics of the joints.

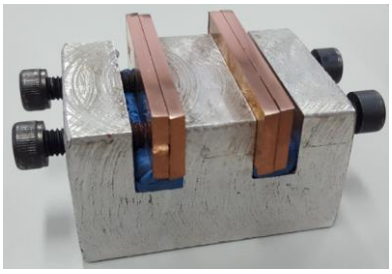

Fig. 6.5.5. Device for orienting and fixing the specimens

6.6. Macroscopic and microscopic analysis

The macrostructural and microstructural analysis of the joints was performed with the help of optical microscopes with a magnification capacity of up to 500 times.

The shape and dimensions of the specimens (Fig. 6.6.1) were adopted taking into account the data identified in the literature [G01] and the recommendations of the specialists from the research center where the experiments were performed (ISIM Timișoara).

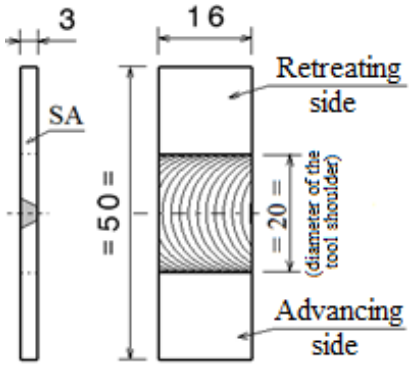

Fig. 6.5.4. Shape and dimensions of specimens for macrostructure analysis, microstructure analysis and microhardness measurement

6.7. Welding bead roughness measurement

A portable digital roughness meter, MAHR PS-10, was used to measure roughness. The roughness of FSW joints is largely influenced by the deformation's characteristic of FSW welding processes made by the shoulder of the active element on the surface of the parts (the effect of "onion rings"). In view of this aspect, the roughness measurement was performed in three areas of the specimen, in a direction parallel to the welding direction, as indicated in Fig. 6.7.1.

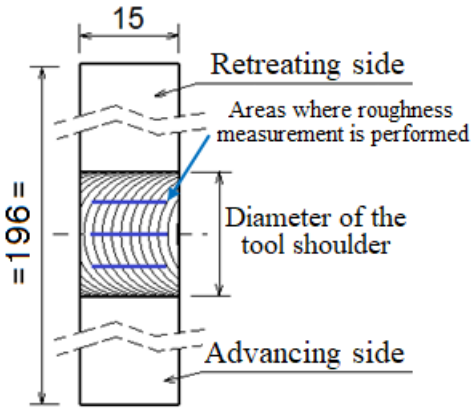

Fig. 6.7.1. Areas of specimens in which the roughness of the weld bead is measured

6.8. Microhardness measurement

The determination of Vickers microhardness was performed with the help of an electronic device for measuring the microhardness type InnovaTest Falcon 500 [V02].

The values of the Vickers microhardnesses of the welded joints were determined in cross section, under a load of 0,3 kgf (2,94 N) and a penetration time of 10 s, positioned at a distance of 1 mm from each other, at half the thickness of the welded parts (Fig. 6.8.2).

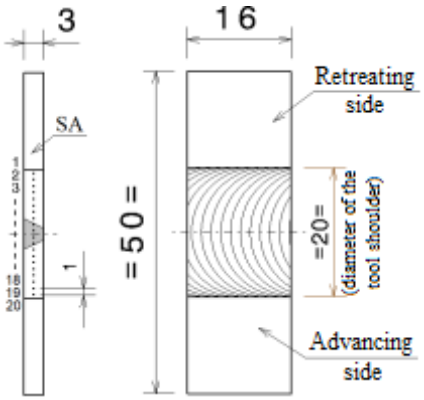

Fig. 6.8.2. Position of points for measuring microhardness

6.9. Tensile test

Tensile tests were performed within ENSTA Bretagne, on a hydraulic tensile test machine type INSTRON 1342 (Fig. 6.9.2), according to the standard SR EN ISO 6892-1.

Each specimen (Fig. 6.5.2) was elongated along its main axis at a constant speed of 8 mm/min until it broke. During the test, the load (force) borne by the specimen and its deformation (strain, extension) were measured. These data were used to determine the tensile strength, R_m, and the percentage total extension at fracture of the joints, A_t, according to the following relations:

$$R_m = \frac{F_m}{S_0} \text{ [MPa]} \qquad A_t = \frac{\Delta L_f}{L_e} 100 \text{ [\%]}$$

where: F_m is the maximum force supported by the specimen, S_0 - the area of the initial cross-section of the calibrated zone of the specimen, ΔL_f - elongation/ extension at fracture and L_e - the basic length of the extensometer.

Knowing the heterogeneous structure of these joints and the fact that the determination of local stresses and strains, on each area of the joint, is briefly addressed in the literature (see § 2.6), in these researches some specimens were tested in traction using the Digital Image Correlation method.

The determination of the extension and strain fields and the determination of their evolution on the two perpendicular faces of the specimens (frontal and lateral - prepared as described in § 6.5) were made using two CCD cameras simultaneously, synchronized with the tensile test machine (Fig. 6.9.2).

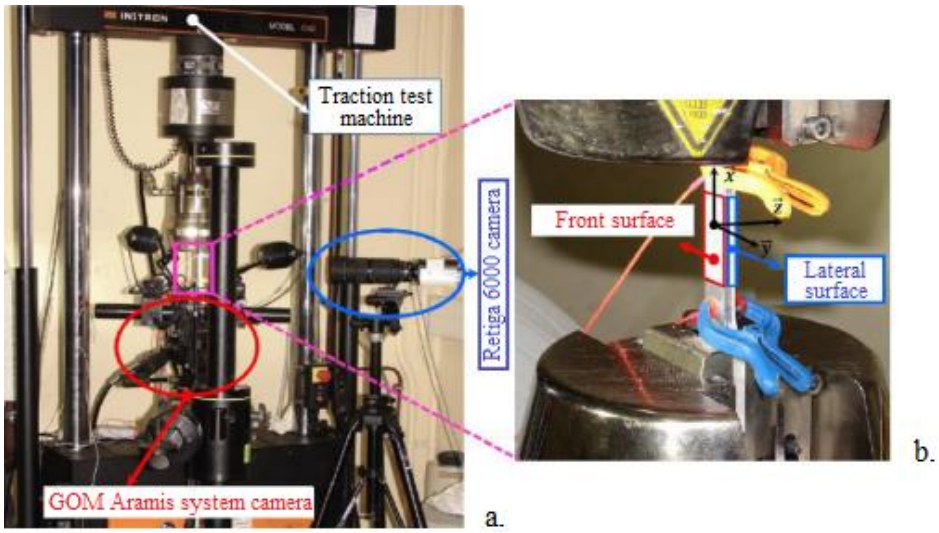

Fig. 6.9.2. Working system for tensile testing and digital image correlation: (a) overview,
(b) detail of the area of freckles on the front and side surfaces of the tested specimen (see also Fig. 6.5.3)

Chapter 7. Results of the preliminary theoretical-experimental research on friction stir welding processes with rotating active element without or with additional heat input of some Cu-DHP structures

Results of the preliminary theoretical-experimental research on Hybrid Friction Stir Welding of some copper structures, which also include published elements of the author [C15, C16, C17, C18, N03, S10], are presented below.

7.1. General data regarding the development of the preliminary theoretical-experimental research program

Within the preliminary experimental plan, the experiments presented in Tables 5.3.2 - 5.3.3 were performed, for the butt welding of Cu-DHP using the FSW process, respectively FSW-TIG. Of these experiments, two failed (2.1 and 2.2) because the joined structures could not be detached from the table of the FSW welding machine without breaking the joint.

The coding, preparation and characterization of the specimens sampled from the welded structures (Fig. 7.1.1) was performed according to the methods and means of sampling, coding, preparation and characterization previously established (see § 6.1-6.8).

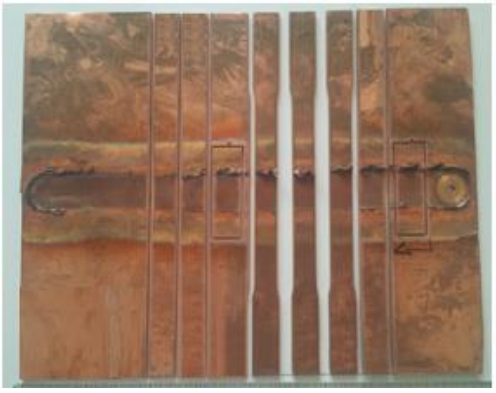

Fig. 7.1.1. Image of a welded structure in the preliminary research (exp. 1.1) and of the specimens sampled from it

7.2. Axial process force and process temperature

The evolution of the temperature and that of the axial force were represented on the same diagram, superimposed over the sampling scheme of the specimens from the welded structure (Fig. 7.2.3). This mode of representation allowed highlighting the local process conditions in which the joint was made, respectively, the conditions associated with the areas from which the specimens were sampled, as well as highlighting the moment when the axial force becomes approximately constant during the experience (the time from which the process becomes stable).

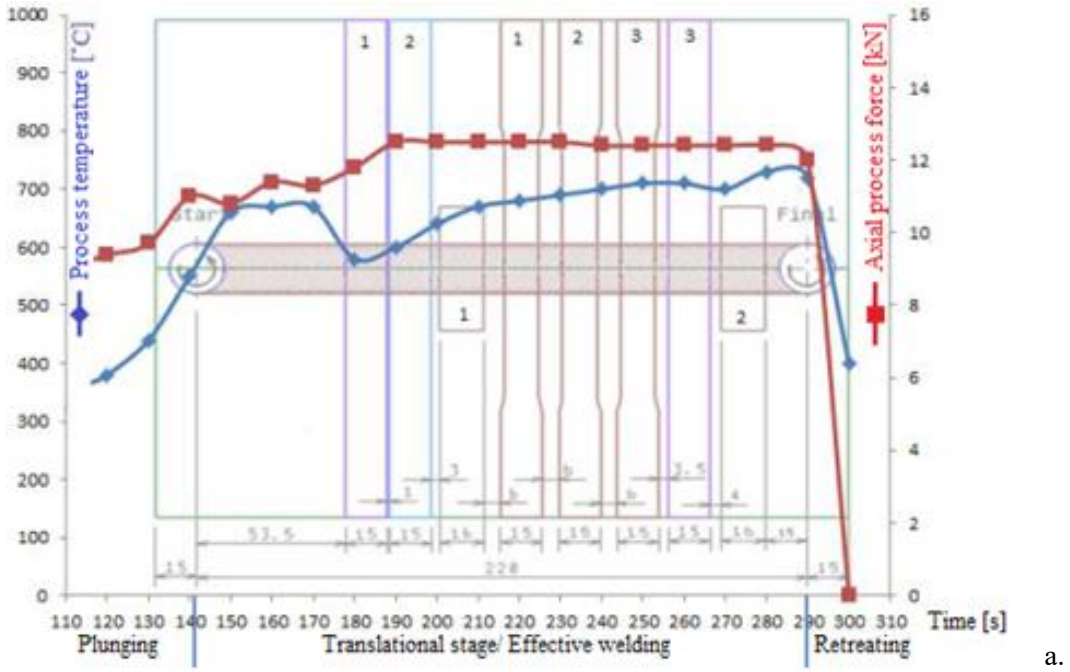

a.

b.

Fig. 7.2.3. Process temperature, axial process force (a) and the aspect of the welded joint (b) at FSW welding - exp. 1.1 (n = 1200 rpm, w = 90 mm/min)

Analysis of the evolutions of temperature and axial force from the diagrams of the type presented in Fig. 7.2.3 highlights a number of dependencies. The following is emphasized.
- The highest temperature is found, as expected, in experiments using the FSW-TIG hybrid procedure (Table 7.6.1).
- The temperature generated in the FSW and FSW-TIG processes increases with increasing active element rotational speed, axial process force and/or decreasing welding speed.
- The axial process force plays a very important role in the realization of free defects FSW joints. From Fig. 7.2.3 it is observed, comparing the evolution of the axial force with the aspect of the welded joint, that channel and insufficient penetration defects are eliminated only after the increase of the axial process force.

7.3. Exterior surfaces, macrostructure and microstructure of welded joints

The upper surface of the FSW and FSW-TIG welding beads has a succession of circular marks specific to these types of joints, due to the contact between the shoulder of the active element and the material to be welded (Fig. 7.3.1).

The visual inspection of the joints highlighted, for some specimens, the existence on the face of the welding beads of some of the defects presented in the literature, such as channel defects, insufficient penetration and excessive burr (Fig. 7.3.1).

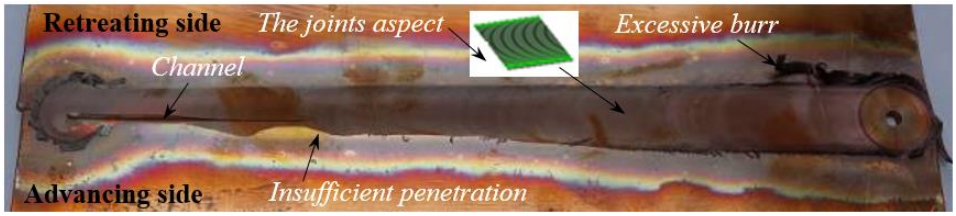

Fig. 7.3.1. The aspect and surface defects of FSW and FSW-TIG joints

The channel-type defect occurs, in particular, in the first part of the joint and is caused by the lack of consolidation of the material on the advancing side (Fig. 7.2.3). For the experiments performed, this defect was mostly eliminated in the second half of the joint, by gradually increasing the required axial process force.

Insufficient penetration defect usually occurs in the first part of the joint and is also a consequence of the application of insufficient axial process force (Fig. 7.3.1). This defect is characterized by a decrease in the width of the circular marks specific to FSW joints at dimensions smaller than the shoulder diameter of the active element.

Excessive burr defect (Fig. 7.2.3, 7.3.1) is caused by the joint being made in too hot working conditions. Analyzing the process temperatures of the joints that have excessive burrs, we notice that they have the highest average values recorded in the preliminary research, values that exceed 650 ˚C (Table 7.6.1).

The macroscopic analysis was performed in the cross section of the joint, as shown in § 6.6, on the specimens dedicated to this analysis (Fig. 6.4.1), prepared as shown in § 6.5. The macroscopically investigated area comprises the entire thickness of the welded plates and a width of approximately 5 mm of the weld bead, arranged symmetrically with respect to the joint line (Fig. 7.3.2). Representative images with the macrostructure of a FSW joint and a FSW-TIG joint are presented in Tables 7.3.1, 7.3.2. These images show a 15x magnification of the real situation.

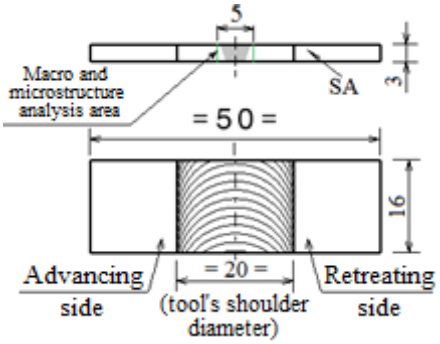

Fig. 7.3.2. Macro and microstructure analysis area

Macrostructural analysis highlights the existence of some defects inside the weld beads, such as tunnel type defects or kissing bond (entrapped oxide particles line) type defects (see § 2.7).

Table 7.3.1. Macrostructure of FSW joints

Exp. 1.3	
Epv. 1.3.1	Epv. 1.3.2
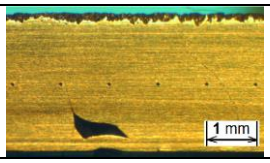	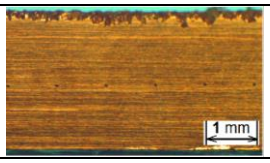

Table 7.3.2. Macrostructure of FSW-TIG joints

Exp. 2.3	
Epv. 2.3.1	Epv. 2.3.2
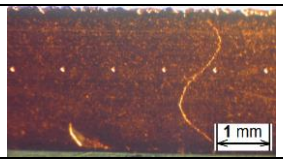	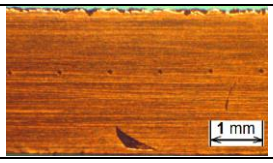

Comparing the macrostructures of the two specimens sampled from the same joint structure, it was found that the specimens sampled at the end of the joint no longer show the defects identified on the specimens sampled from the first part of the joints or that they are diminished (Table 7.3.1). This justifies sampling as many specimens as possible from the second part of the joints.

The microstructure analysis was performed on the same two specimens on which the macrostructural analysis of these structures was performed (Fig. 6.4.1), prepared as presented in § 6.5.

Microscopic examination of the welds obtained by the conventional FSW procedure (exp. 1.5 and 1.6), in connection with the characteristic areas of a FSW joint, highlights the following aspects (Fig. 7.3.4).

• The base material (BM) has a structure composed of polyhedral grains.
• The nugget zone (NZ) has small grains, strongly deformed and with diffuse borders compared to those of the BM. This structure of the grains is a consequence of the high level of plastic deformations recorded in this area, which reduced the effect of heat flux.
• The thermo-mechanically affected zone (TMAZ) has less deformed grains, with clear borders and larger in size than those found in the NZ, but smaller than those of the BM.
• In the heat affected zone (HAZ), the grains are larger than those of the BM, because this area is no longer subject to mechanical deformations, but only to the thermal flow which has as a consequence the increase of the grain size [C15, L04].

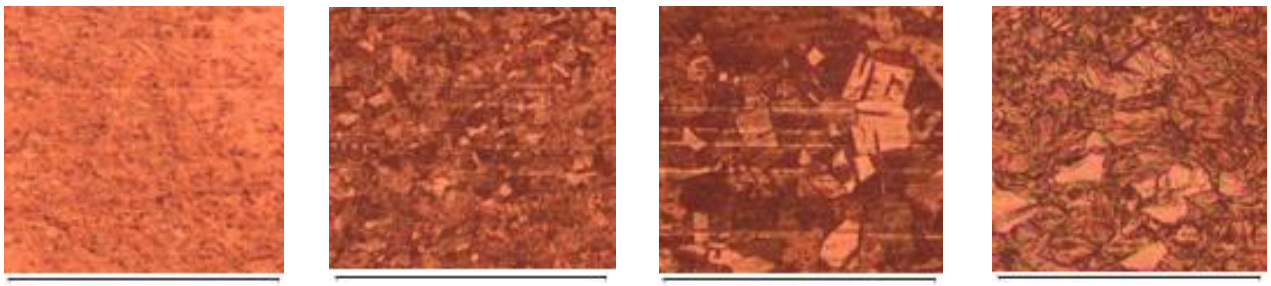

100 µm NZ (200x) | 100 µm TMAZ (200x) | 100 µm HAZ (200x) | 100 µm BM (200x)

Fig. 7.3.4. Microstructure of the FSW welded structures 1.5 and 1.6

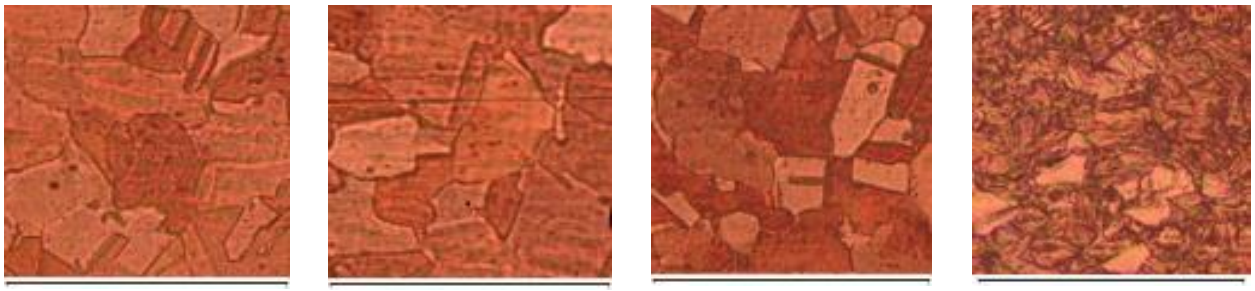

100 µm NZ (200x) | 100 µm TMAZ (200x) | 100 µm HAZ (200x) | 100 µm BM (200x)

Fig. 7.3.5. Microstructure of the FSW-TIG welded structure 2.3

Microscopic examination of the weld obtained by the FSW-TIG hybrid procedure (exp. 2.3), in connection with the characteristic areas of an FSW joint, highlights the following aspects (Fig. 7.3.5).

• In all areas of the weld bead, the grain size is larger than that of the BM grains.

• The microstructure of the joint has slightly deformed grains in the NZ area, larger than those found in the BM. This aspect of the grains represents the effect of the thermal field which reduced the effect of the important mechanical deformations achieved in this area.

• TMAZ has, to a large extent, the same microstructural characteristics as NZ, which makes the boundary between these two areas practically imperceptible for the FSW-TIG hybrid process.

• In HAZ, the structure has the specific characteristics of a high temperature, which leads, in addition to the beginning of recrystallization, to an increase in grain size, larger than those in BM, but smaller than those in NZ and TMAZ [C15].

The grain sizes in the macrostructural areas specific to the FSW and FSW-TIG joints are presented comparatively in the extended version of this paper.

7.4. Welding bead roughness

The roughness of the welding bead, an important feature of it, was measured as shown in § 6.7, respectively, on three specimens for each welded structure (Fig. 6.4.1). The measurements were performed on the welding direction, for each specimen being performed three measurements, according to those presented in Fig. 6.7.1.

The lowest values of the Ra roughness (below 1 μm) correspond to the experiences in which the lowest temperatures were recorded during the FSW process (below 500 ºC), respectively the experiments 1.2, 1.5 and 1.6. The highest values of Ra roughness (of ~ 4 μm) were obtained for exp. 2.3, the FSW-TIG experience in which the highest temperature was recorded during the process.

7.5. Microhardness of welded joints

The microhardness of the welded joints, their important characteristic, was measured as presented in § 6.8, respectively, on two specimens for each welded structure (Fig. 6.4.1), prepared according to those presented in § 6.5. The measurements were performed transversely to the welding direction, according to those shown in Fig. 6.8.2.

For the comparative analysis of the microhardnesses corresponding to the two specimens from the same welded structure (specimens sampled from different areas of the joint/ with different local process conditions), as well as for an easier comparison of the microhardnesses in the advancing side with those in the retreating side, the profiles of the microhardnesses of the two specimens of each welded structure were reunited on the same diagram (Fig. 7.5.7, 7.5.12).

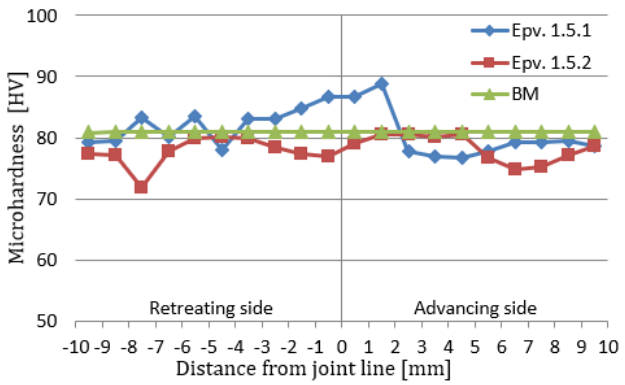

Fig. 7.5.7. Microhardness profiles of the specimens 1.5.1 and 1.5.2 (exp. 1.5)

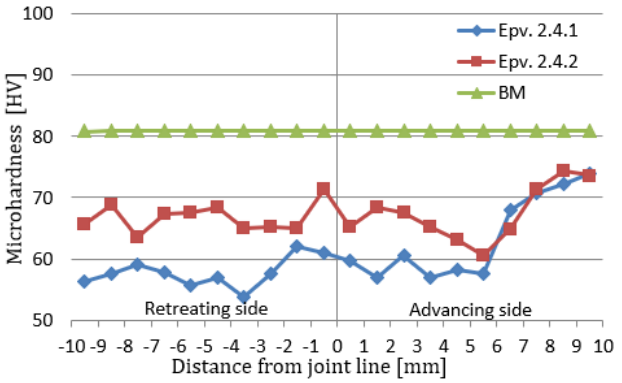

Fig. 7.5.12. Microhardness profiles of the specimens 2.4.1 and 2.4.2 (exp. 2.4)

From the analysis of the 20 microhardness profiles it was found that the generation of high temperatures in the process leads to a softening annealing and, consequently, to a decrease in the joint microhardness [C01, C16, S06, S17, X01]. Thus, the lowest values of microhardness were obtained for the structures welded by the hybrid process (Fig. 7.5.12), in which the process temperature had the highest values (Table 7.6.1). The decrease in the amount of heat during the process leads to a refinement of the grain size and thus to a high microhardness of the welds, equal to or even greater than that of the base material (Fig. 7.5.7).

Regarding the dependence of the microhardness profile on the local process conditions registered at the level of each specimen, the following conclusions can be drawn.

- No significant differences are identified between the microhardness values of the specimen sampled from the beginning of the joint and those of the specimen sampled from its end when the axial force and temperature values in the process are approximately equal in the two areas associated with the analyzed specimens.

- The values of the microhardnesses of the specimen sampled from the beginning of the joint are higher than those of the specimen sampled from the end of the joint (Fig. 7.5.7) when the process temperatures are lower at the beginning of the joint and higher at the end.

- The values of the microhardnesses of the specimen sampled from the beginning of the joint are lower than those of the specimen sampled from the end of the joint (Fig. 7.5.12), although the values of the process temperature in the two areas are approximately equal or even higher for the specimens sampled from the end of the joint when the cooling rates on the two areas associated with the analyzed specimens are different, respectively, the second specimen cools faster.

7.6. Tensile strength and percentage total extension at fracture

The tensile strength of welded joints, their important characteristic, was measured as shown in § 6.9, respectively, on three specimens for each welded structure (Fig. 6.4.1), prepared in advance according to the data presented in § 6.5.

The tensile strength of the specimens has higher values for the specimens of the structures obtained by the classical FSW process and lower values for the specimens of the structures obtained by the FSW-TIG process.

By making a correlation between the values of the temperature in the process and those of the tensile strength, it is observed, as in the case of microhardness, that with increasing temperature the tensile strength decreases (Table 7.6.1). It is found that the three highest values of tensile strength are obtained for structures made in experiments in which the average process temperature is in the range 466 - 500 °C.

The percentage total extension at fracture is, for most of the joints made, much lower than that of the base material, whose value is 55 %.

A synthesis comprising the average values of temperature, axial force, tensile strength, extension at fracture and microhardness, associated with the processes and structures experienced in the 10 experiments performed in the preliminary research is presented in Table 7.6.1. From this table we can identify, with relative ease, the experimental conditions that led to the best properties of welded joints, properties that are largely closely related to the average temperatures recorded during the process.

Table 7.6.1. Average values of the axial process force, process temperature, microhardness, tensile strength and extension at fracture, depending on the technological parameters

Exp. code	Rotati-onal speed	Welding speed	TIG source intensity	Axial process force	Process temperature		Micro-hardness		Tensile strength		Extension at fracture	
	n	w	I	F_z*	T*		HV*		R_m*		A_t*	
	[rpm]	[mm/min]	[A]	[kN]	[˚C]	C	[HV]	C	[MPa]	C	[%]	C
1.1	1200	90	-	12.5	693	8	66.6	8	193.2	4	4.4	3
1.2	1000	90		9.7	466	1	80.4	2	218.6	1	25.2	1
1.3	1200	150		11.8	580	6	71.8	6	190.5	5	9.1	2
1.4	1000	150		13.2	550	5	79.9	3	171.3	7	1.5	8
1.5	800	90		12.6	476	2	79.6	4	216.6	2	2.5	5
1.6	800	150		12.6	500	3	81.1	1	207.4	3	1.6	7
1.7	1000	120		9.1	530	4	74	5	165.6	8	2.1	6
1.8	1000	120		11.6	663	7	68.3	7	189.5	6	4.3	4
2.3	1000	250	100	11.7	868	10	62.7	10	135.8	10	0.7	10
2.4	1000	350		12	845	9	63.9	9	147.8	9	1.2	9
Base material (Cu-DHP)							**81**		**257**		**55**	
Legend FSW exp.: 1.1, 1.2, ..., 1.8; FSW-TIG exp.: 2.3, 2.4; *: Average of acceptable values, C: Ranking												

7.7. Case study on the presence and influence of some defects in welded structures

A case study was performed to highlight some defects of FSW welded structures and their influence on the behavior of specific specimens, based on data recorded during the tensile test and Digital Image Correlation (see § 6.5, 6.9, 7.3, 7.6, [S10]), as follows.

It was analyzed a group of specimens sampled from the welded structures made in exp. 1.2 and 1.4, as well as from the base material (BM). During the tensile test of a specimen (see § 6.9), are considered the true stress, σ_v, and the true strain, ε_v, respectively:

$$\sigma_v = \sigma(1+\varepsilon),\ \varepsilon_v = \ln(1+\varepsilon),\ \sigma = F/S_0,\ \varepsilon = \Delta L/L_0,\ \Delta L = L - L_0 \qquad (7.7.2)$$

where: σ and ε are the conventional stress and, respectively, the conventional strain [R05]; S_0 and L_0 - the area of the initial cross-section and, respectively, the initial length/ distance between two marks associated with the calibrated zone of the specimen; F - load force; ΔL - extension of the specimen; L - the length of the calibrated zone of the specimen on which the extension is measured at any time during the test [S18];

For each specimen, the relation/ dependence between the average true stress, $\overline{\sigma_v}$, and the average true strain, $\overline{\varepsilon_v}$, is determined. For the considered specimens, the resulting graphical dependencies are as shown in Fig. 7.7.1 [S10].

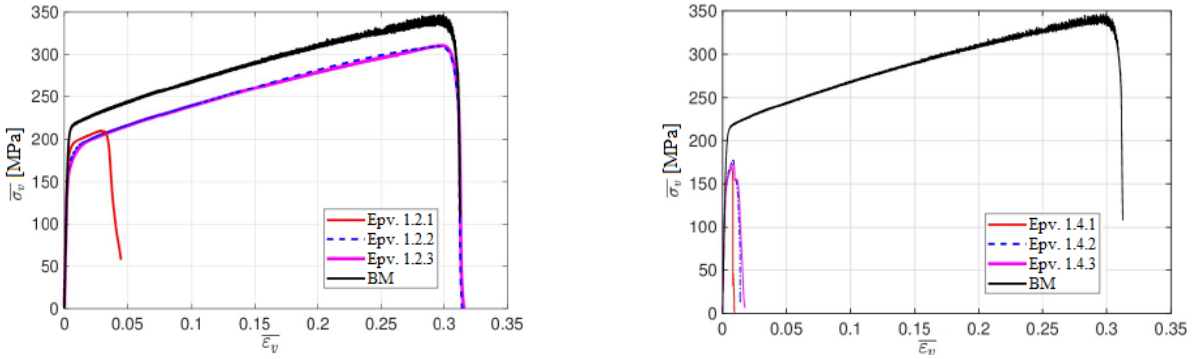

a. Epv. 1.2.1, 1.2.2, 1.2.3, BM b. Epv. 1.4.1, 1.4.2, 1.4.3, BM

Fig. 7.7.1. Relations between the average true stress, $\overline{\sigma_v}$, and the average true strain, $\overline{\varepsilon_v}$

Overall, it can be observed that, compared to the FSW welded structure 1.2, the FSW welded structure 1.4 presents a lower maximum stress $\overline{\sigma_v}$ by about 44 %.

In relation to the above, in-depth analysis of Epv. 1.2.3 and Epv. 1.4.3 (sampled from the stability zone of the welding process) is performed and are considered the relations ($\overline{\sigma_v}$, $\overline{\varepsilon_v}$) for small values, 0 - 0,015, of the average true strain $\overline{\varepsilon_v}$, respectively:

$$\overline{\sigma_v} = f_v(\overline{\varepsilon_v}),\ \overline{\varepsilon_v} \in [0;\ 0{,}015) \qquad (7.7.4)$$

The resulting graphical dependencies (rel. 7.7.4) are as shown in Fig. 7.7.4. It is also considered a series of working values of $\overline{\sigma_v}$ during the tensile test and the corresponding states ($\overline{\sigma_v}$, $\overline{\varepsilon_v}$) of Epv. 1.2.3 and Epv. 1.4.3, as shown in Fig. 7.7.4.

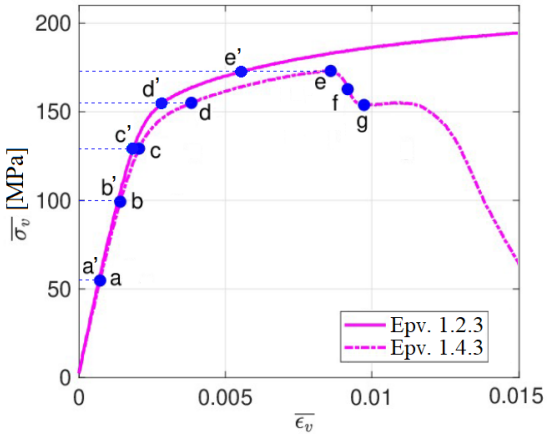

Fig. 7.7.4. The relations between the average true stress, $\overline{\sigma_v}$, and the average true strain, $\overline{\varepsilon_v}$, for small values of the $\overline{\varepsilon_v}$, at Epv. 1.2.3 and Epv. 1.4.3

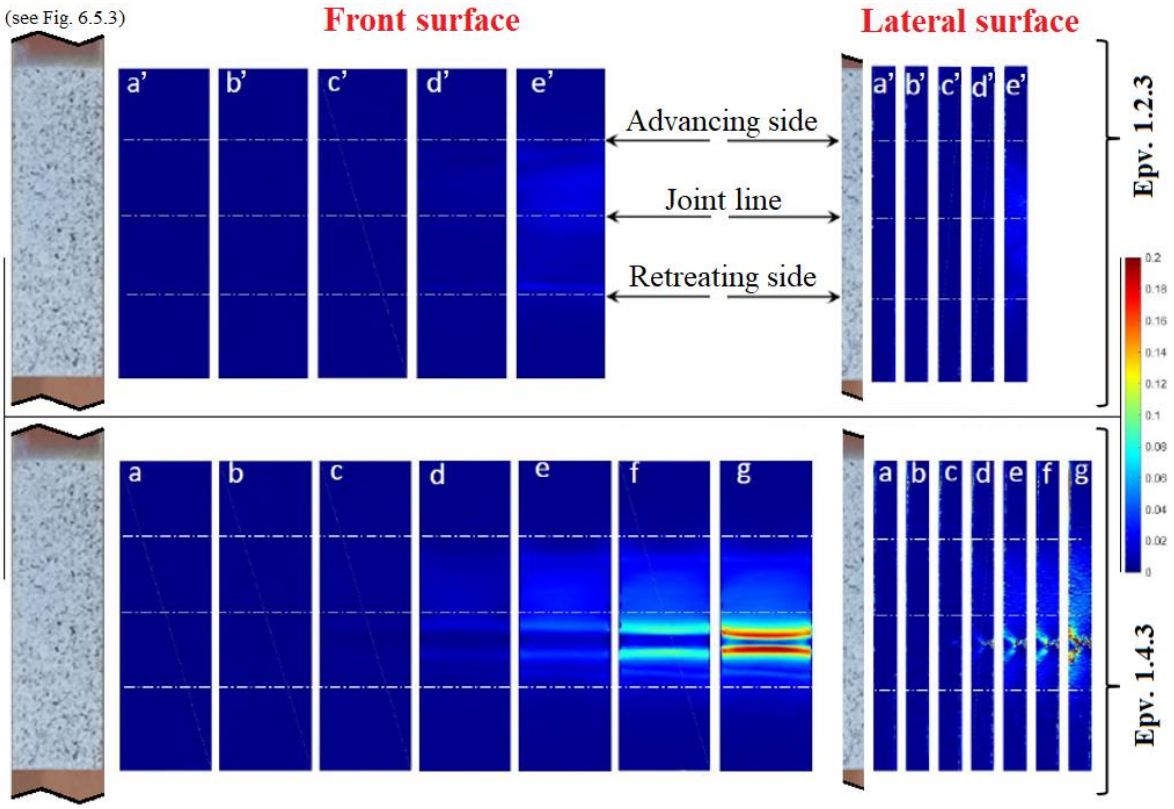

Fig. 7.7.6. The true strain maps/ fields corresponding to the states *a′, b′, ..., e′* and *a, b, ..., g* of Epv. 1.2.3 and Epv. 1.4.3, at traction in x direction (see also Fig. 6.9.2)

For each state *a′, b′, ..., e′* and *a, b, ..., g* the extension field/ map (see the extended version of this paper) and the true strain field/ map (Fig. 7.7.6) associated with the freckles from the front and lateral surfaces of Epv. 1.2.3 and Epv. 1.4.3 are determined by processing the data recorded during the tensile test and the digital image correlation.

The differences between the true strain fields associated with states *d′* and *d*, *e′* and *e* and their evolution for states *f* and *g* indicate that Epv. 1.4.3 breaks to a tensile stress and a strain lower than those recorded at Epv. 1.2.3 (see § 7.6, Fig. 7.7.1.a, b, 7.7.4).

In addition, at Epv. 1.4.3, the true strain fields highlight, starting from the state *d* of the lateral surface (Fig. 7.7.6), the localization of more severe true strains that have "butterfly" shape, a shape specific to a field of strains generated around a crack. Taking into account that also on the retreating side of the joint, near the contact zone between the conical surface of the rotating active element and the welded material, the kissing bond defect was identified (see also § 7.3), the appearance of this crack is attributed to the presence of this defect.

7.8. Orientation of advanced research

The mechanical properties of FSW and FSW-TIG copper joints are negatively influenced by the increase in process temperature. Preliminary research results and some studies identified in the literature [H07] show that the best mechanical properties are obtained in experiments in which the average temperatures during the process are in the range 460 - 530 °C.

Consequently, in order to obtain lower temperatures during the FSW-TIG process and thus improve the mechanical properties of the obtained joints, while maintaining the high productivity of this process, in advanced research it is necessary to carry out interventions on the values of technological parameters. Thus, from the analysis of the preliminary research results that the feasible options for lowering the process temperature are represented by the decrease of the rotational speed of the active element and the decrease of the additional heat input generated by the TIG source [C18].

Chapter 8. Results of the advanced theoretical-experimental research on friction stir welding processes with rotating active element without or with additional heat input of some Cu-DHP structures

Results of advanced theoretical-experimental research on Hybrid Friction Stir Welding of some copper structures, which also include published elements of the author [C18], are presented below, grouped by the quantities analyzed during research, which characterizes the FSW/ FSW-TIG welding process and the welded structure.

8.1. General data regarding the development of the advanced theoretical-experimental research program

Considering the conclusion of the preliminary theoretical-experimental research, according to which the feasible options for lowering the process temperature, at values leading to good mechanical properties of welded structures by the FSW-TIG process, are represented by the decrease of the active element rotational speed and the decrease of the additional heat input generated by the TIG source, the experiments presented in Tables 5.3.4 - 5.3.5 were proposed and performed for the butt welding of Cu-DHP using the FSW process, respectively FSW-TIG.

Fig. 8.1.1. Image of a welded structure in advanced research (exp. 2.10) and of the specimens sampled from it

The coding, preparation and characterization of the specimens sampled from the welded structures (Fig. 8.1.1) was performed according to the methods and means of sampling, coding, preparation and characterization previously established.

8.2. Axial process force and process temperature

Temperature and axial force were measured using the means given in § 6.2. As in the case of preliminary research, the measured values of temperature and axial force were represented on the same diagram, superimposed over the sampling scheme (Fig. 8.2.10).

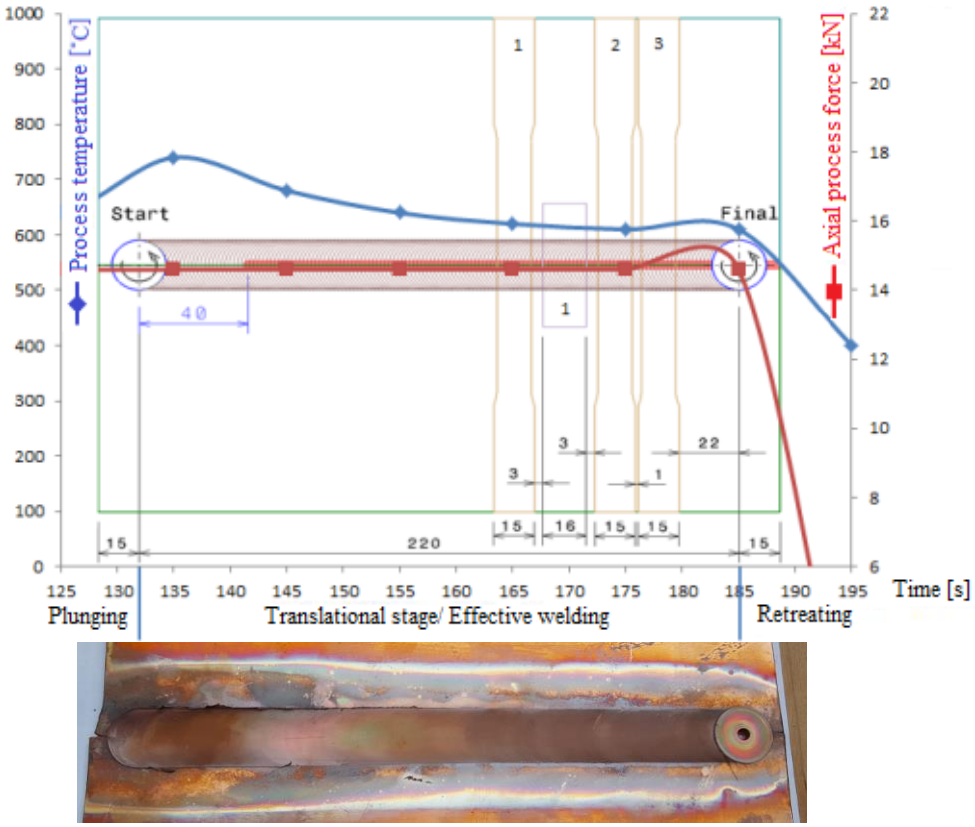

a.

b.

Fig. 8.2.10. Process temperature, axial process force (a) and aspect of the welded joint (b) at FSW-TIG welding - exp. 2.10 (n = 1000 rpm, w = 250 mm/min, I = 80 A)

Analysis of the variation of temperature and axial force values in the previous diagrams highlights a number of dependencies. The following is emphasized.

- The process temperatures recorded in the FSW experiments, presented in Table 8.6.1, show values included or very close to the target range, 460 - 530 °C.

- The temperatures recorded in the FSW-TIG process decreased compared to those recorded in the preliminary experiments (Table 8.6.1), reaching values much closer to the above-mentioned range. This fact indicates the correct choice of the values of the technological parameters in the advanced researches, ensuring the necessary premises to fulfill the established objective.

- Axial process force (pressing force) has a very important role in the defect-free realization of FSW and FSW-TIG joints, especially in cases where a set of technological parameters is used that lead to insufficient material mixing:

$$\frac{\textbf{\textit{Low}}\ \textit{rotational speed}\ [\text{rpm}]}{\textbf{\textit{High}}\ \textit{welding speed}\ [\text{mm/min}]} = \textbf{\textit{Low}}\ \textit{mixing rate}\ [\text{rot/mm}] \Rightarrow \textbf{\textit{Insufficient mixing}}$$

- Thus, in the experiments performed, once the welding speed is increased, it is also necessary to increase the axial force, to compensate for this mixing deficit.

- Due to the decrease of process temperatures in these experiments, it is observed that the defects of excessive burr type are greatly diminished.

8.3. Exterior surfaces and macrostructure of welded joints

The macroscopic analysis was performed in the cross section of the joint, on the specimens dedicated to this analysis (Fig. 6.4.2), using an optical microscope with a 15x magnification of the taken image. The macroscopically investigated area has the same location as the one macroscopically analyzed in the preliminary research (Fig. 7.3.2). Representative images with the macrostructure of FSW/ FSW-TIG joints are presented in Tables 8.3.1, 8.3.2.

Table 8.3.1. Macrostructure of FSW joints

Exp. 1.11	Exp. 1.12
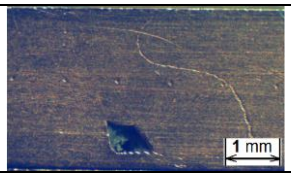	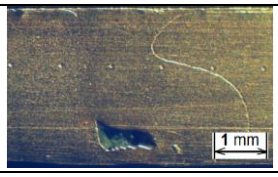

Table 8.3.2. Macrostructure of FSW-TIG joints

Exp. 2.8	Exp. 2.10
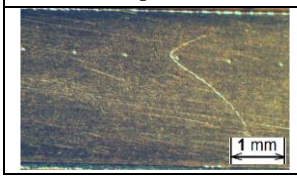	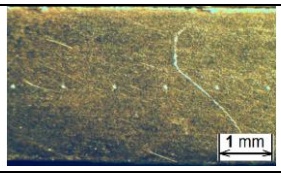

The macrostructural analysis highlights the existence of tunnel and kissing bond type defects inside the weld beads. This analysis allowed the location of these defects according to the trajectory followed by the active element (Fig. 8.3.1) and the identification of the causes of their generation, which are presented in the extended version of this paper.

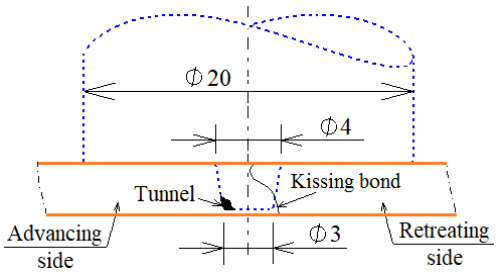

Fig. 8.3.1. Position of some defects at FSW and FSW-TIG joints

The only joints performed in advanced research that do not show the tunnel defect are the FSW-TIG joints 2.8 and 2.10. It is observed that the welded structure in exp. 2.8 shows the characteristics of a strong joint (average process temperature in the range 460 - 530 °C and the absence of the tunnel defect).

8.4. Welding bead roughness

The roughness of the weld bead, an important feature of it, was measured as shown in § 6.7. If in the preliminary research the roughness was measured on specimens dedicated exclusively to this analysis, this time the measurements were made on the specimens for the tensile test, before their test (see § 6.4).

From the analysis of the average roughness values determined at the level of each welded structure it is found that the lowest roughness values correspond to the welding beads made in the experiments with the lowest temperatures recorded in the process (FSW/ FSW-TIG) (Fig. 8.4.3). Therefore, as the temperature generated during the process increases, the resistance to plastic deformation of the welding material decreases and, consequently, the joint surface has higher roughness [C17].

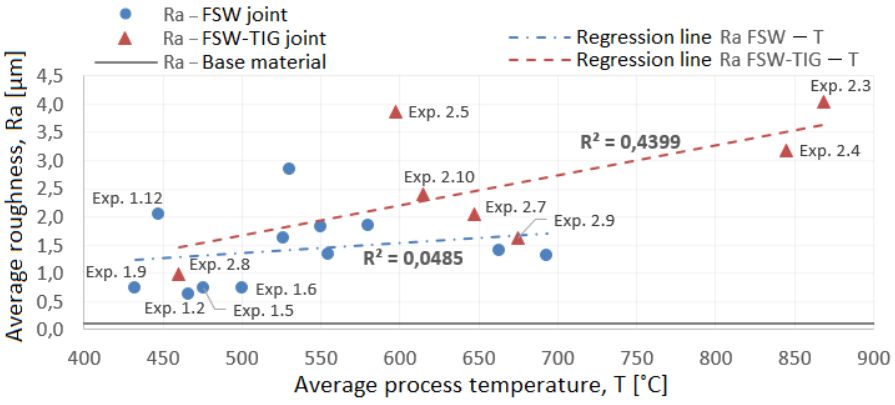

Fig. 8.4.3. Elements of the regression analysis regarding the correlation between the welding bead roughness and the average process temperature

8.5. Microhardness of welded joints

The microhardness of the welded joints, their important characteristic, was measured as shown in § 6.8, respectively, on a specimen for each welded structure (Fig. 6.4.2), prepared in advance according to the data presented in § 6.5.

The profiles of the microhardnesses of the welded structures in the advanced research were grouped in a single diagram, for each process, FSW (Fig. 8.5.1) and FSW-TIG (Fig. 8.5.2). The analysis of the two diagrams shows the superiority of the classical FSW process over the hybrid one in terms of the resulting microhardnesses in the joint area.

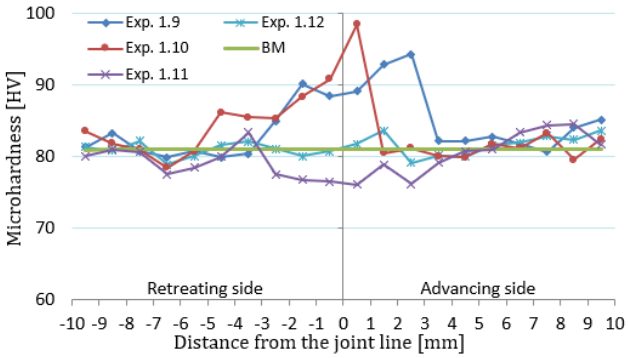

Fig. 8.5.1. The microhardness profiles of FSW welded structures

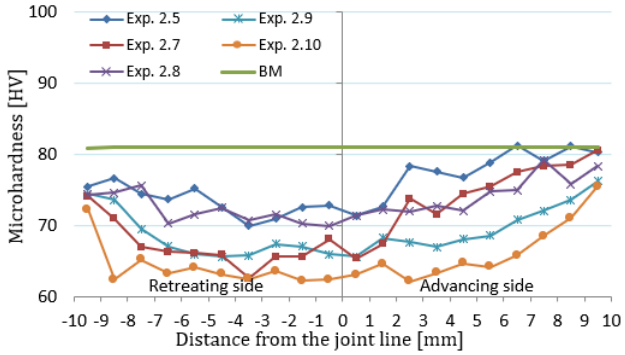

Fig. 8.5.2. The microhardness profiles of FSW-TIG welded structures

The negative slope of the regression lines generated based on the average values of the microhardnesses of the FSW and FSW-TIG joints also indicates the decrease of the microhardness with the increase of the temperature registered in the process (Fig. 8.5.3). The relatively high values of the coefficients of determination R^2 indicate that the microhardness of the joints is strongly influenced by the temperature variation.

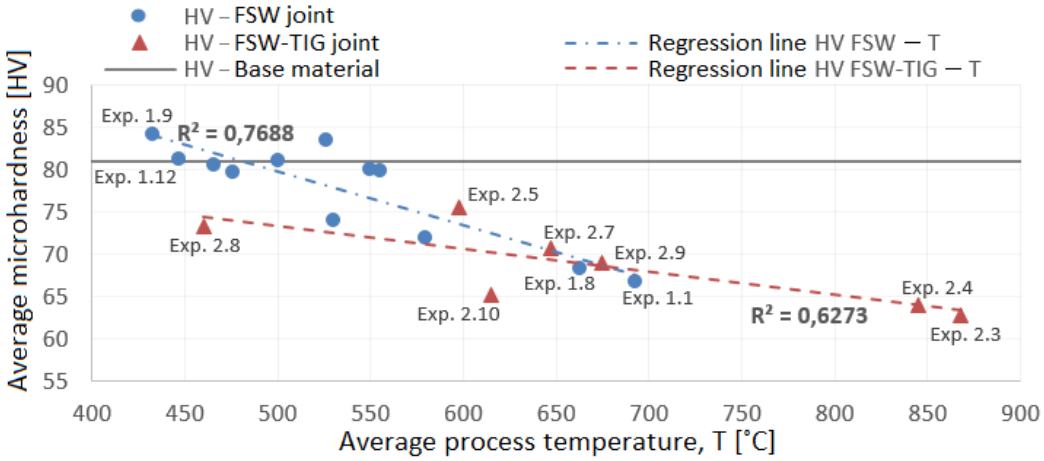

Fig. 8.5.3. Elements of the regression analysis regarding the correlation between the average joint microhardness and the average process temperature

The comparative analysis of the microhardnesses determined on the specimens made in the preliminary researches and of those determined on the specimens made in the advanced researches, highlights the fact that the microhardnesses of the welded structures in the advanced researches have higher values than those obtained in the preliminary researches. This is due to the decrease in temperatures recorded in these experiments (Table 8.6.1). For FSW joints, there was a 4 % increase in microhardness compared to the microhardness of the base material, and for FSW-TIG joints, an increase of up to 93 % from the microhardness of the base material.

8.6. Tensile strength and percentage total extension at fracture

The tensile strength of welded joints, their important characteristic, was measured as shown in § 6.9, respectively, on three specimens for each welded structure (Fig. 6.4.2), previously prepared according to the data presented in § 6.5.

A synthesis that includes the average values of tensile strengths of the specimens sampled from the welded structures in the advanced research is presented in Table 8.6.1.

Table 8.6.1. Average values of the axial process force, process temperature, microhardness, tensile strength and extension at fracture, depending on the technological parameters

Exp. code	Rotational speed	Welding speed	TIG source intensity	Axial process force	Process temperature		Micro-hardness		Tensile strength		Extension at fracture	
	n	w	I	F_z*	T*		HV*		R_m*		A_t*	
	[rpm]	[mm/min]	[A]	[kN]	[˚C]	C	[HV]	C	[MPa]	C	[%]	C
1.9	800	90	-	10.1	432.5	1	84.2	1	186.8	3	2.8	3
1.10	800	120		13.1	526	3	83.4	2	179.8	4	1.5	4
1.11	800	120		14.4	555	4	79.8	4	197.6	2	4.5	2
1.12	800	150		15.9	447	2	81.2	3	200.6	1	4.7	1
2.5	800	350	100	21	597.5	3	75.5	1	186.3	4	2.8	4
2.6	800	350		15.5	553	2	-	-	-	-	-	-
2.7	800	250		21	647.5	5	70.7	3	190.1	3	4.1	3
2.8	800	250		19.2	460	1	73.2	2	235.1	1	35.8	1
2.9	1000	350	80	20.4	675	6	68.9	4	150.9	5	1	5
2.10	1000	250		14.6	615	4	65.1	5	222.6	2	15	2
Base material (Cu-DHP)							**81**		**257**		**55**	

Legend
FSW exp.: 1.9, 1.10, 1.11, 1.12; FSW-TIG exp.: 2.5, 2.6, ..., 2.10; *: Average of acceptable values, C: Ranking

Considerable improvements have been made in the tensile strengths of FSW-TIG welded structures in advanced research, reaching up to 91,5 % of the tensile strength of the base material. This percentage is higher than the highest percentage obtained for structures joined by the FSW process, of 85,1 % of the tensile strength of the base material.

This considerable increase in the tensile strength of welded structures is due to the decrease in temperatures in the hybrid process, in the context of maintaining a good mixing of the material in the weld bead. This proper mixing is characterized by a uniform visual aspect of the weld bead and the absence of defects, both on the face of the bead and in its section. Thus, it can join the main advantage of the FSW-TIG process, represented by its increased productivity, and the possibility of making joints of pure Cu with superior mechanical properties, similar to those made using the classic FSW process.

The negative slope of the regression lines generated based on the average values of tensile strengths measured on specimens sampled from structures welded by FSW and FSW-TIG processes indicates the same trend of decreasing the tensile strength with the increase of the temperature recorded in the process (Fig. 8.6.3).

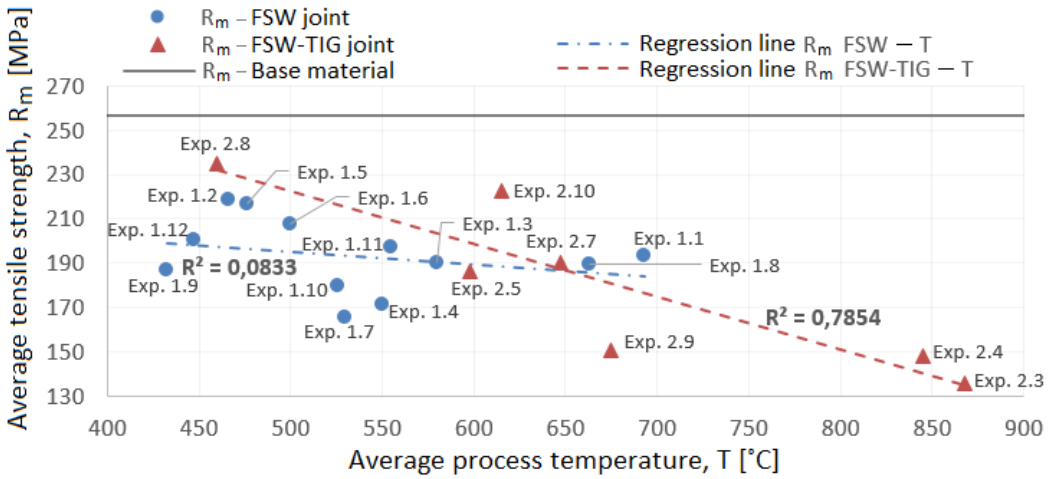

Fig. 8.6.3. Elements of the regression analysis regarding the correlation between the tensile strength of welded structures and the average process temperature

It is observed that four of the five highest values of tensile strength were obtained in experiments in which the average process temperatures are in the range 460 - 530 °C (Table 8.6.1, Fig. 8.6.3). The highest average value of tensile strength is identified for the welded structure in exp. 2.8, FSW-TIG experience in which the lowest average process temperature was recorded. The lowest values of tensile strength are those of welded structures in the FSW-TIG experiments, 2.3 and 2.4, experiments in which the highest average process temperatures were recorded (Fig. 8.6.3). As these structures had a proper visual aspect, both on the front of the cord and in cross section, superior to other structures, it is estimated that the low values of tensile strength are caused by the high amount of heat generated in these experiments.

The percentage total extension at fracture of welded structures remains, for most experiments, much lower than that of the base material ($A_{t\ BM}$ = 55 %). The only welded structures for which an extension at fracture of more than 5 % was registered are those made in: exp. 2.8 - A_t = 35,8 %, exp. 1.2 - A_t = 25,2 %, exp. 2.10 - A_t = 15 % and exp. 1.3 - A_t = 9,1 %. It follows that for most welds the rupture was brittle, while ductile fractures characterized the strongest welds (Table 8.6.1).

Therefore, the highest average value of the extension at fracture reaches 65,1 % of the extension at fracture of the base material. This was obtained, as in the case of tensile strength, for the welded structure in exp. 2.8, the FSW-TIG experience in which the lowest average process temperature was recorded, between 460 - 530 °C.

Chapter 9. Numerical modeling and simulation of friction stir welding process with rotating active element of some Cu-DHP structures

The development of a valid numerical model using the CEL formulation, for the FSW joint of two pieces of pure copper and the results obtained using this model, which also include published elements of the author [C13, C14, C19, C20], are presented as follows.

9.1. Development of the numerical model

During the research, a thermo-mechanically coupled three-dimensional numerical model of the FSW process was developed for the butt welding of two pure copper plates using the CEL (Coupled Eulerian-Lagrangian) formulation and Abaqus 6.13 software. The CEL formulation is one of the few formulations capable of modeling such large deformations as those found in FSW processes.

To develop the numerical model, the following activities were performed: reproducing the geometry of the constituent elements, defining the behavior of the material and the type of contact between the surfaces, establishing the boundary conditions (Fig. 9.1.1) and discretizing the constituent elements. These activities are presented in more detail in the extended version of this paper.

The technological parameters used for the development of this numerical model are identical to those used in exp. 1.6 (preliminary experience of the FSW process). The reason for choosing this experiment is that it used the highest welding speed and obtained the welded structure with the best mechanical tensile strength. The welding speed is the technological parameter that, both at the experimental level, but especially at the level of numerical simulation, considerably reduces the duration of the development/ calculation of the process.

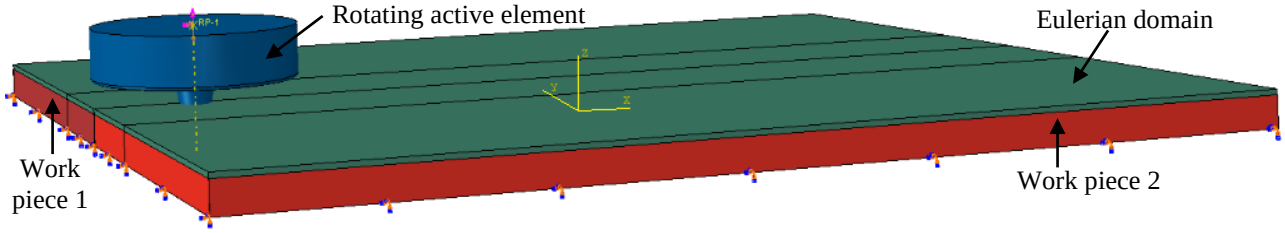

Fig. 9.1.1. Boundary conditions of the numerical model in Abaqus/ Explicit

9.2. Numerical simulation results

Validation of the numerical model

It can be observed that, in the plunging stage, the temperature is distributed symmetrically with respect to the joint axis (Fig. 9.2.1). These results are similar to those identified in the literature [L03] and to the experimental data resulting from the visual analysis of the distribution of the thermally affected area in the area of penetration of the active element (Fig. 9.2.2).

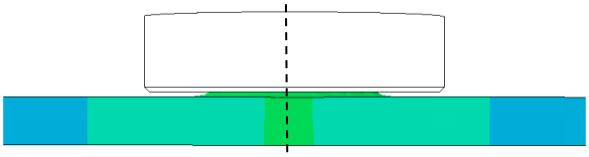

Fig. 9.2.1. Temperature distribution in the plunging stage (computational time 0,8 s)

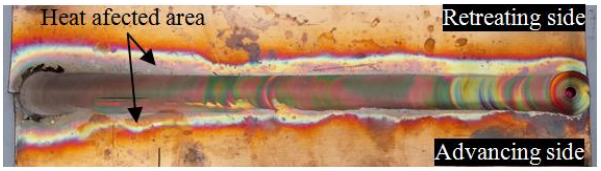

Fig. 9.2.2. The aspect of the FSW joint at exp. 1.6

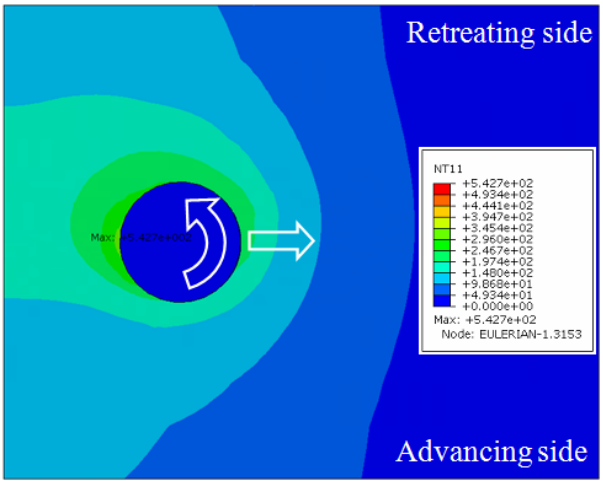

Fig. 9.2.3. Temperature distribution in the translation/ effective welding stage (computational time 8 s)

In the effective welding stage, the temperature field has a slight asymmetry (Fig. 9.2.3). The temperature is higher on the retreating side of the joint compared to the advancing side, due to the larger amounts of material that are entrained on this side [J01, K02, P03]. This higher temperature on the retreating side, during the translation stage, is also highlighted in the experimental results (Fig. 9.2.2).

The maximum nodal temperatures estimated by numerical simulation, at 20 mm and 50 mm, respectively, at the beginning of the translation stage are approximately 542 ºC (Fig. 9.2.3) and 530 ºC, respectively. These values are close to the experimentally determined temperatures, of approximately 525 °C at 20 mm and 500 °C at 50 mm from the beginning of the translation stage, respectively.

An important disadvantage of the CEL formulation is the extremely long computational time. Therefore, in order to reduce this disadvantage, a strategy to reduce the computational time was used, a strategy which is presented below.

Applying the mass-scaling strategy to reduce computational time

The mass scaling strategy reduces the computational time by artificially increasing the mass of the material (its density) [L08, R02]. Thus, the density used in the numerical model and implicitly in determining the critical time increment, Δt_{crit}, is scaled by replacing the value of the density ρ with a fictitious density $\rho^* = \kappa_m \rho$, where κ_m (mass scaling factor) > 0.

To investigate the effect of mass scaling, four values of mass scaling factor, κ_m, were used: $\kappa_m \in [1,\ 10^2,\ 10^3\ and\ 10^4]$. Fig. 9.2.7.a shows the evolution of the axial process force during the plunging stage, considered as an indicator as to the adequacy of the mass scaling factor, κ_m, used, in the sense that the smoother the evolution of this process characteristic, therefore the mass scaling factor, κ_m, is considered more appropriate. As expected, a constant evolution of the axial process force is obtained for $\kappa_m = 1$. For values of the mass scaling factor $\kappa_m \geq 100$ we can observe a degradation of the smoothness of the evolution of the axial process force. However, the determined values of the axial force for $\kappa_m \geq 100$ remain, on average, quite close to those obtained without mass scaling.

The distribution of the temperature field is compared in Fig. 9.2.7.b for its different values along the joint line, at 11,05 s from the start of the translation stage. It can be noticed that there are differences between the temperature distributions, mainly in the vicinity of the pin of the active element (Fig. 9.2.7.b). The increase in temperature with the increase in the value of the mass scaling factor, κ_m, is explained by the fact that a higher density of the material generates a higher local plastic deformation, due to the inertia of the material, and higher contact pressures, which increase the amount of heat generated by friction.

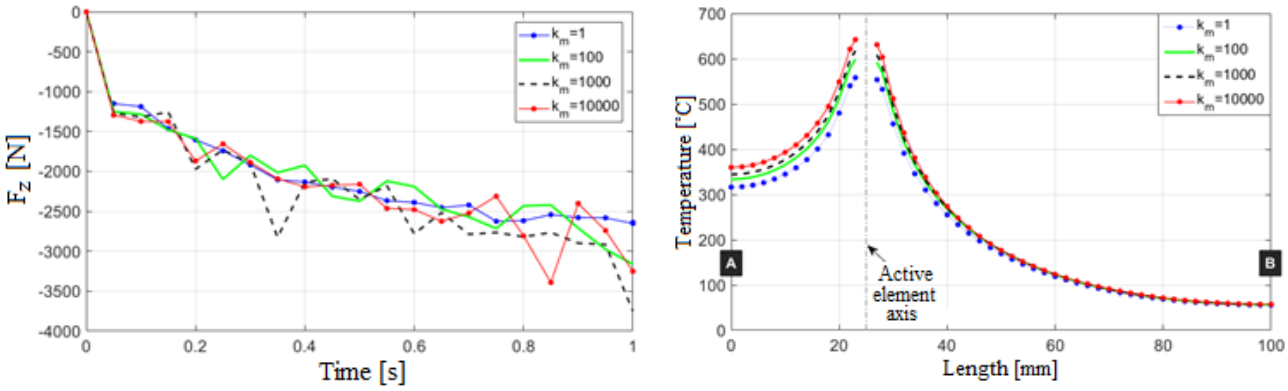

a. b.

Fig. 9.2.7. The effect of the mass scaling on: (a) the evolution of the axial process force, F_z, during the plunging stage, (b) the distribution of the temperature field on the joint line (AB)

The recorded error related to the temperatures calculated in the simulations with values of $\kappa_m > 1$ is shown in Fig. 9.2.8. It is determined in the vicinity of the pine, where the differences between the calculated temperatures are the largest. It is observed that this error in determining the temperature field is proportional to the parameter κ_m.

Also, in Fig. 9.2.8 is represented the influence of the mass scaling factor, κ_m, on the computational time. There is a significant decrease in the computational time as the κ_m increases.

In conclusion, the mass scaling strategy introduced to reduce the computation time of the numerical simulation is effective. It has been shown that the computational time of the numerical simulation can be significantly reduced, with a slight degradation of the obtained results. Thus, this approach can be used for parametric studies, necessary to improve the FSW process, or to simulate other complex industrial applications.

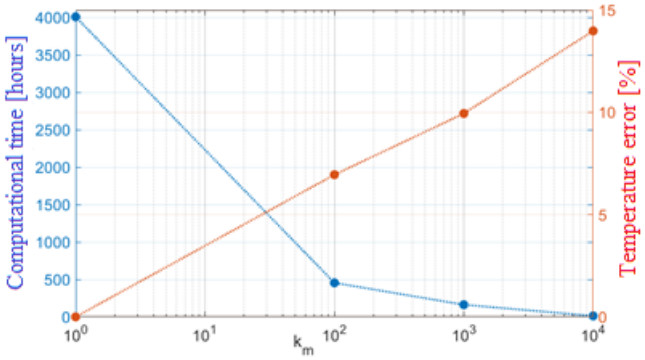

Fig. 9.2.8. The evolution of the computational time and the error of determining the process temperature according to mass scaling factor, κ_m

Chapter 10. Final conclusions and main contributions to the development and numerical modeling of friction stir welding processes and systems with rotating active element without or with additional heat input of some Cu-DHP structures

(1) From the analysis of the current state of research and development and industrial applications on Hybrid Friction Stir Welding of copper structures, important conclusions have been drawn, which are presented in chapter 4.

(2) Considering the data from the analysis of the current state of research-development of the Hybrid Friction Stir Welding of the copper structures, the research-development directions presented in § 5.1 were considered to be topical.

(3) In relation to the current state and the research-development directions regarding the Hybrid Friction Stir Welding of some copper structures, it was assumed as main objective of the research-development activity within the doctorate (see and § 5.2): development, through theoretical-experimental research and numerical modeling, of friction stir welding processes and systems with rotating active element without or with additional heat input of some copper structures.

(4) The relevant conclusions regarding the doctoral research and development activity for achieving its main objective, noted from the preliminary theoretical-experimental research carried out according to the chosen research-development methodology (see § 5.3), are as follows:

○ The temperature recorded in the FSW and FSW-TIG processes increases with increasing rotational speed of the active element, with increasing axial force and reducing the welding speed, thus respecting the laws of variation presented in the literature. The axial process force plays a very important role in the defect-free realization of FSW and FSW-TIG joints (see § 7.2).

○ The macrostructural analysis revealed the existence of some defects inside the weld beads, such as tunnel type defects or kissing bond type defects. It is also noted that the specimens sampled from the end of the joint no longer show the defects identified on the specimens sampled from the first part of the joints or that these defects are diminished. This is justified by the stabilization of the process in the second part of the joint and certifies the correct sampling of as many specimens as possible from the second part of the joints (see § 7.3).

○ The decrease in grain size is due to the decrease in temperature and the increase in deformations recorded in the experiments. The joints that showed small grain sizes also showed good mechanical properties. Due to the fact that all macrostructural areas characteristic of FSW joints (NZ, TMAZ, HAZ) have very close temperatures, the generation of different microstructural areas identified at the specimen level is due to the distribution of plastic deformations (see § 7.3).

○ The temperature recorded in the process has a defining role in the variation of the joint roughness values. As it grows, the material of the parts is slightly deformed and, consequently, the face of the weld beads has higher roughness (see § 7.4).

○ Increasing the amount of heat during the welding process leads to a softening annealing of the material and thus to a decrease in its microhardness. Reducing the amount of heat leads to a reduction in the size of the grains and, consequently, to an increased microhardness of the joints, equal to or even greater than that of the base material. A variation of the microhardness of the joints was also observed depending on their cooling rate, in the sense that the increase of the cooling rate of the area from which the specimen dedicated to this analysis was sampled, leads to the increase of the obtained microhardnesses, similar results being identified in the literature (see § 7.5).

○ The tensile strength of welded specimens has higher values, close to those of the base material, for the FSW process and lower values for the FSW-TIG hybrid process. The increase above a certain temperature limit recorded in the process, encountered in the case of FSW-TIG experiments, leads to significant decreases in the values of tensile strength. The percentage total extension at fracture has, for most experiments, values much lower than that of the base material (see § 7.6).

○ A new strategy for identifying kissing bond type defects using the method of Digital Correlation of Images on two perpendicular faces of a FSW or FSW-TIG welded specimen is presented in these researches. This defect is clearly highlighted by the displacement field on the side face, which allows the identification of displacements in the thickness of the joint, thus capturing the propagation of the crack depending on the applied mechanical stress (see § 7.7).

○ It is highlighted as a general conclusion of the preliminary theoretical-experimental researches that the microstructural and mechanical properties of FSW and FSW-TIG joints of copper are negatively influenced by the increase in temperature recorded in the process. Thus, in the advanced theoretical-experimental research, some modifications of the technological parameters were made in order to obtain lower temperatures and thus improve the values of mechanical properties of FSW-TIG joints, while maintaining the high productivity of these processes (see § 7.8).

(5) The relevant conclusions regarding the doctoral research and development activity for achieving its main objective, noted from the advanced theoretical-experimental research carried out according to the research-development methodology, by performing the aforementioned interventions on technological parameters (see § 8.1), are as follows:

○ The temperatures recorded in the FSW-TIG process were lower, reaching values close to or included in the target range. During this interval, according to the results of preliminary theoretical-experimental research and certain data identified in the literature, good mechanical properties are obtained when joining pure copper using the FSW process (see § 8.2).

○ The axial forces used in advanced experimental research were higher than those in preliminary experimental research, having a very important role in the defect-free realization of FSW and FSW-TIG joints made with these technological parameters (low rotational speeds and high welding speeds). They must make up for the deficiency in the mixing of the material caused by the low value of the ratio between the rotational speeds and the welding speeds used (see § 8.2).

○ Macrostructural analysis highlights the existence of the same types of defects that have been identified in the case of preliminary joints. The analysis of all the joints made highlights the fact that the tunnel type defect is found on the advancing side of the weld bead, while the kissing bond type defect is found in the vast majority of cases on its retreating side. However, there are also situations in which it has a small passage in the advancing side (see § 8.3).

○ The way of variation of the roughness of the joints, highlighted in the preliminary theoretical-experimental researches, is also identified in the case of the advanced ones. Thus, the FSW-TIG experience in which the lowest values of temperature and roughness were obtained is exp. 2.8. The measured average value of roughness, of 0,98 μm, is comparable to the lowest average value obtained by the classical FSW process, of 0,62 μm, for the welded structure in exp. 1.2 (see § 8.4).

○ The microhardnesses of the joints made in the advanced theoretical-experimental researches have higher values than those made in the preliminary researches, behavior justified by the decrease of temperatures recorded in these experiments. The microhardness analysis of all joints indicates a close variation of this characteristic depending on the temperature generated in the process. For the FSW procedure, in exp. 1.9 there was an increase of 4 % over the microhardness of the base material, and for the FSW-TIG process, in exp. 2.5 there was an increase of up to 93 % from the microhardness of the base material (see § 8.5).

○ As in the case of microhardness, with increasing temperature, the tensile strength decreases. However, the temperature dependence of the tensile strength is not as close as that of the microhardness. Obtaining the best tensile properties is not guaranteed by generating a low temperature under any conditions, but by generating these low temperatures by using a set of technological parameters that achieve a good mixing of the material in the weld bead. This good blending is characterized by a uniform visual aspect, without defects, both on the front of the cord and in its section. Thus, the indices that characterize a FSW or FSW-TIG joint with good mechanical properties are:

- the visual aspect specific to these joints on the face of the cord (the width of the circular marks equal to the diameter of the shoulder of the active element),
- the temperature recorded in the process between 460 and 530 ˚C,
- absence of tunnel defects in the joints section (see § 8.6).

○ The experience from which resulted the highest average value of tensile strength is exp. 2.8 (FSW-TIG experience), obtaining 91,5 % of the tensile strength of the base material. We can thus combine the main advantage of the FSW-TIG process, represented by its increased productivity, and the possibility of making welds of pure copper with superior mechanical properties, similar to those made using the classical FSW process (see § 8.6).

○ The percentage total extension at fracture has much lower values for most experiments than the base material. The highest average value of the extension at fracture, of 65,1 % of the extension at fracture of the base material, resulted, as in the case of tensile strength, for the welded structure in exp. 2.8. It follows that, for most welded structures, the rupture was brittle, while ductile fractures characterize the strongest welds (see § 8.6).

(6) In achieving the main objective of the doctoral research-development activity, this doctoral thesis brings a series of contributions, of which the most important are as follows.

• Determining by theoretical-experimental research some process characteristics and some characteristics of the FSW and FSW-TIG joints of copper for which, in some situations, contradictory data are indicated in the literature.

• Identification of the conditions for the realization of a FSW-TIG joint of pure copper without defects, with a productivity at least twice higher than that of the FSW process and with good mechanical properties, respectively: 91,5 % of the tensile strength of the base material, 65,1 % of the extension at fracture of the base material and 90,4 % of its microhardness.

• Presentation of a new strategy for identifying defects inside FSW or FSW-TIG welded joints, using during the tensile test the Digital Image Correlation method on two of the four perpendicular faces of the welded specimen.

• Development of a thermo-mechanically coupled three-dimensional numerical model of the FSW process for butt welding of two pure copper plates using the CEL (Coupled Eulerian-Lagrangian) formulation, able to simulate the FSW joining of pure copper plates and determine the temperature distribution in welding bead.

*** * ***

This doctoral thesis, through issues, approach and results, develops knowledge of the process of copper welding by Hybrid Friction Stir Welding generated by a TIG source and indicates the possibility of using this process with remarkable results for joining this material.

The scientific importance of this doctoral thesis is supported by the contributions to determine the dependencies of process characteristics and properties of welded joints by the technological parameters of the FSW/ FSW-TIG process, to the joining of copper structures. These contributions also aim at developing a valid numerical model for simulating the FSW butt joining process of a copper structure.

The practical importance of this doctoral thesis lies in the fact that it presents the research methodology, research methods and means of FSW and FSW-TIG processes applied to the joining of copper structures, which is a system - useful support for students, teachers, organizations and specialists.

The issue of studying FSW processes requires a research and development activity continuous and analytical, to determine the local mechanical behavior, on each area of the joint by exploiting the method of Digital Image Correlation, to determine the fields of displacement and strains that are generated during tensile test.

As future research directions, it can be considered to increase the values of rotational speed and welding speed in the FSW-TIG experiments, keeping constant the value of the ratio between them (3 - 4 rot/mm), in an attempt to obtain the highest possible productivity. It is also possible to improve the current numerical model to explore the capabilities of the CEL formulation on identifying defects in FSW joints and extend it to the analysis of the FSW-TIG process, in order to provide a relevant means of research, evaluation and development of these processes.

References

[A03] F. Al-Badour, M. Nesar, S. Abdelrahman, A. Bazoune, *Coupled Eulerian Lagrangian finite element modeling of friction stir welding processes*, J. of Materials Processing Technology 213 (2013) 1433-1439.

[A04] A. Ali, M. Brown, C. Rodopoulos, S. Gardiner, *Characterization of 2024-T351 friction stir welding joints*, J. of Failure Analysis and Prevention 6 (2006) 83-96.

[A05] M. Al-Moussawi, *A Mathematical and Experimental Analysis of Friction Stir Welding of Steel*, Doctoral Thesis, Sheffield Hallam University, 2018.

[A06] C.G. Andersson, R.E. Andrews, *Proceedings of the First Int'l Symposium on Friction Stir Welding*, 1999, Thousand Oaks, USA.

[A09] P. Asadi, R.A. Mahdavinejad, S. Tutunchilar, *Simulation and experimental investigation of FSP of AZ91 magnesium alloy*, Materials Science and Engineering A 528 (2011) 6469-6477.

[A10] M. Assidi, L. Fourment, S. Guerdoux, T. Nelson, *Friction model for friction stir welding process simulation: Calibrations from welding experiments*, Int'l J. of Machine Tools & Manufacture 50 (2010) 143-155.

[A11] H.J. Aval, S. Serajzadeh, A.H. Kokabi, *Experimental and theoretical evaluations of thermal histories and residual stresses in dissimilar friction stir welding of AA5086-AA6061*, Int'l J. of Advanced Manufacturing Technology 61 (2012) 149-160.

[B01] N. Balasubramanian, B. Gattu, R.S. Mishra, *Process forces during friction stir welding of aluminium alloys*, Science and Technology of Welding and Joining 14 (2009) 141-145.

[B03] H. Bang, H.J. Song, S.M. Joo, *Joint properties of dissimilar Al6061-T6 aluminum alloy / Ti-6%Al-4%V titanium alloy by gas tungsten arc welding assisted hybrid friction stir welding*, Materials and Design 51 (2013) 544-551.

[B05] G.F. Batalha, A. Farias, R. Magnabosco, S. Delijaicov, M. Adamiak, L.A. Dobrzański, *Evaluation of an AlCrN coated FSW tool*, J. of Achievements in Materials and Manufacturing Engineering 55 (2012).

[B06] J.M. Benjamin, *Welding of Copper Alloys*, https://www.slideshare.net/JabinMathewBenjamin/welding-of-copper-alloys (accessed on 12.08.2019).

[B07] I. Boromei, L. Ceschini, A. Morri, G.L. Garagnani, *Friction stir welding of aluminium based composites reinforced with Al2O3 particles: effects on microstructure and charpy impact energy*, Metallurgical Science and Technology 24(1) (2006) 12-21.

[B08] A. Boșneag, **M.A. Constantin**, E. Nițu, *Numerical simulation of Friction Stir Welding of three dissimilar aluminium alloys*, Materials Science and Engineering 564 (2019) DOI: 10.1088/1757-899X/564/1/012033 (Innovative Manufacturing Engineering and Energy Int'l Conference, IManEE 2019, Pitești, România) *[Volum ISI]*.

[B13] A. Boșneag, **M.A. Constantin**, E. Nițu, M. Iordache, D. Iacomi, *Study on Analysis between Friction Stir Welding Process and Hybrid Friction Stir Welding Process*, Annals of the „Constantin Brâncuși" University of Târgu-Jiu, Engineering Series(3) (2015) 59-65 (Conferință științifică națională cu participare internațională, CONFERENG 2015, Târgu-Jiu, România) *[Revistă BDI]*.

[B14] A. Boșneag, **M.A. Constantin**, E. Nițu, M. Iordache, A. Rizea, *Friction Stir Welding of Composite Materials with Metallic Matrix: a Brief Review*, Applied Mechanics and Materials 809-810 (2015) 449-454, DOI: 10.4028/www.scientific.net/AMM.809-810.449 (Innovative Manufacturing Engineering Int'l Conference, IManE 2015, Iaşi, România) *[Volum BDI]*.

[B15] G. Buffa, J. Hua, R. Shivpuri, L. Fratini, *A continuum-based FEM model for friction stir welding-model development*, Materials Science and Engineering A 419 (2006) 389-396.

[C01] G. Cam, *Friction Stir Welded Structural Materials: Beyond Al-Alloys*, Int'l Materials Reviews 56 (2011) 1-48.

[C02] D. Campanella, C. Casavola, A. Cazzato, L. Fratini, V. Moramarco, C. Pappalettere, *Residual Stress Measurement in Innovative FSW Processes*, Key Engineering Materials 754 (2017) 391-394.

[C03] S.L. Campanelli, G. Casalino, C. Casavola, V. Moramarco, *Analysis and Comparison of Friction Stir Welding and Laser Assisted Friction Stir Welding of Aluminium Alloy*, Materials 6 (2013) 5923-5941.

[C06] C. Casavola, A. Cazzato, V. Moramarco, *Residual Stress in Friction Stir Welding and Laser - Assisted Friction Stir Welding by Numerical Simulation and Experiments*, IntechOpen (2018).

[C12] R. Cojocaru, C. Ciucă, L. Boţilă, V. Verbiţchi, *FSW-TIG Welding of Cu 99 Copper*, Welding and Material Testing (2015).

[C13] **M.A. Constantin,** A. Boşneag, M. Iordache, C. Bădulescu, E. Nițu, *Numerical Simulation of Friction Stir Spot Welding*, Applied Mechanics and Materials 834 (2016) 43-48, DOI: 10.4028/www.scientific.net/AMM.834.43 (Int'l Conference on Advanced Manufacturing Technologies, ICAMaT 2015, Bucharest, România) *[Volum BDI]*.

[C14] **M.A. Constantin**, A. Boşneag, M. Iordache, E. Nițu, D. Iacomi, *Numerical Simulation of Friction Stir Welding of Aluminum Alloys: A Brief Review*, Applied Mechanics and Materials 809-810 (2015) 467-472, DOI: 10.4028/www.scientific.net/AMM.809-810.467 (Innovative Manufacturing Engineering Int'l Conference, IManE 2015, Iaşi, România) *[Volum BDI]*.

[C15] **M.A. Constantin**, A. Boșneag, E. Nițu, L. Boțilă, *Establishing the Dependence of Output Parameters Depending on Local Process Conditions for Friction Stir Welding of Pure Copper Plates*, Advanced Materials Research 1146 (2018) 32-37, DOI: 10.4028/www.scientific.net/AMR.1146.32 (Structural Integrity of Welded Structures, ISCS 2017, Timișoara, România) *[Volum BDI]*.

[C16] **M.A. Constantin**, A. Boșneag, E. Nițu, M. Iordache, *Comparative study on microhardness between friction stir welding and tungsten inert gas assisted friction stir welding of pure copper*, MATEC Web of Conferences 178 (2018) DOI: 10.1051/matecconf/201817803002 (Innovative Manufacturing Engineering and Energy Int'l Conference, IManEE 2018, Chișinău, Republica Moldova) *[Volum ISI]*.

[C17] **M.A. Constantin**, A. Boșneag, E. Nițu, M. Iordache, *Experimental investigations of tungsten inert gas assisted friction stir welding of pure copper plates*, Materials Science and Engineering 252 (2017) DOI: 10.1088/1757-899X/252/1/012038, WOS: 000419817200038 (The Int'l Congress of Automotive and Transport Engineering, CAR 2017, Pitești, România) *[Volum ISI]*.

[C18] **M.A. Constantin**, A. Boșneag, E. Nițu, M. Iordache, *Orientation of process parameter values of TIG assisted FSW of copper to obtain improved mechanical properties*, Materials Science and Engineering 400 (2018) DOI: 10.1088/1757-899X/400/2/022017, WOS: 000461147400017 (Modern Technologies in Industrial Engineering, ModTech 2018, Constanța, România) *[Volum ISI]*.

[C19] **M.A. Constantin**, M. Iordache, E. Nițu, M. Diakhaté, Y. Demmouche, M. Dhondt, C. Bădulescu, *An efficient strategy for 3D numerical simulation of friction stir welding process of pure copper plates*, Materials Science and Engineering 916 (2020) DOI: 10.1088/1757-899X/916/1/012021 (Modern Technologies in Industrial Engineering, ModTech 2020, susținută online, România) *[Volum BDI]*.

[C20] **M.A. Constantin**, E. Nițu, C. Bădulescu, *Numerical simulation of friction stir welding of pure copper plates*, Materials Science and Engineering 564 (2019) DOI: 10.1088/1757-899X/564/1/012031 (Innovative Manufacturing Engineering and Energy Int'l Conference, IManEE 2019, Pitești, România) *[Volum ISI]*.

[D01] P. Dabeera, G. Shindeb, *Perspective of Friction Stir Welding Tools*, Materials Today: Proceedings 5 (2018).

[D02] S. Daftardar, *Laser assisted friction stir welding: finite volume method and metaheuristic optimization*, Thesis, Louisiana State University, 2009.

[D03] A.R. Darvazi, M. Iranmanesh, *Thermal modeling of friction stir welding of stainless steel 304L*, Int'l J. of Advanced Manufacturing Technology 75 (2014) 1299-1307.

[D04] J. De Backer, *Robotic Friction Stir Welding for Automotive and Aviation Applications*, Master Thesis, University West, 2009.

[D05] D. Deheleanu, R. Cojocaru, D. Ionescu, D. Ţurcanu, *Procedeu şi dispozitiv de sudare cu element activ rotitor*, Brevet de invenţie RO 123349, Oficiul de Stat pentru Invenţii şi Mărci, Bucureşti, 2011.

[D06] Y. Demmouche, *Etude du comportement en fatigue d'assemblages soudes par FSW pour applications aeronautiques*, These, École Nationale Supérieure d'Arts et Métiers, 2012.

[F01] K. Fraser, L. St-Georges, L.I. Kiss, *A Mesh-Free Solid-Mechanics Approach for Simulating the Friction Stir-Welding Process*, Joining Technologies 3 (2016).

[F04] H. Fujii, T. Tatsuno, T. Tsumura, M. Tanka, K. Nakata, *Hybrid Friction Stir Welding of Carbon Steel*, Materials Science Forum 580-582 (2008) 393-396.

[G01] R. Gabor, A. Roos, J. Santos, L. Bergmann, *Friction stir welding of AA 5083-H111 alloy*, Welding and Material Testing (2010) 41-48.

[G02] F. Gemme, *Modelisation numerique des phenomenes physiques du soudage par friction-malaxage et comportement en fatigue de joints soudes en aluminium 7075-T6*, These, Ecole Polytechnique de Montreal, 2011.

[G03] C. Genevois, *Genèse des microstructures lors du soudage par friction malaxage d'alliages d'aluminium de la série 2000 et 5000 et comportement mécanique résultant*, Thesis, Institut National Polytechnique de Grenoble, 2004.

[G04] P. Goel, A.N. Siddiquee, N.Z. Khan, M.A. Hussain, Z.A. Khan, M.H. Abidi, A. Al-Ahmari, *Investigation on the Effect of Tool Pin Profiles on Mechanical and Microstructural Properties of Friction Stir Butt and Scarf Welded Aluminium Alloy 6063*, Metals 8(1) (2018).

[G05] K. Gök, M. Aydin, *Investigations of friction stir welding process using finite element method*, Int'l J. of Advanced Manufacturing Technology 68 (2013) 775-780.

[G06] M. Grujicic, G. Arakere, H.V. Yalavarthy, T. He, C.F. Yen, B.A. Cheeseman, *Modeling of AA5083 Material-Microstructure Evolution During Butt Friction-Stir Welding*, J. of Materials Engineering and Performance 19(5) (2010) 672-684.

[G07] M. Grujicic, B. Pandurangan, C.F. Yen, B.A. Cheeseman, *Modifications in the AA5083 Johnson-Cook Material Model for Use in Friction Stir Welding Computational Analyses*, J. of Materials Engineering and Performance 21(11) (2012) 2207-2217.

[H01] C. Hamilton, S. Dymek, A. Sommers, *A thermal model of friction stir welding in aluminum alloys*, Int'l J. of Machine Tools and Manufacture 48 (2008) 1120-1130.

[H04] H. Hori, S. Makita, H. Hino, *Friction stir welding of rolling stock for subway*, FSW Symposium, 1991, USA.

[H06] F.J. Humphreys, M. Hatherly, *Recrystallization of Single-Phase Alloys*, Recrystallization and Related Annealing Phenomena 2(7) (2004).

[H07] Y.M. Hwang, P.L. Fan, C.H. Lin, *Experimental study on friction stir welding of copper metals*, J. of Material Processing Technology 210(12) (2010) 1667-1672.

[J01] M. Jabbari, *Elucidating of rotation speed in friction stir welding of pure copper: Thermal modelling*, Computational Materials Science 81 (2014) 296-302.

[J02] D. Jacquin, B. Meesterb, A. Simarb, D. Deloisonc, F. Montheilleta, C. Desrayauda, *A simple Eulerian thermomechanical modeling of friction stir welding*, J. of Materials Processing Technology 211 (2011) 57-65.

[J03] R. Jain, S.K. Pal, S.B. Singh, *Finite element simulation of temperature and strain distribution in Al2024 aluminum alloy by friction stir welding*, All India Manufacturing Technology Design and Research Conference (2014) 3-7.

[J04] R. Jain, S.K. Pal, S.B. Singh, *Numerical modeling methodologies for friction stir welding process*, Computational Methods and Production Engineering 1(5) (2017) 125-169.

[J05] M. James, M. Mahoney, *Proceedings of the first Int'l Symposium on Friction Stir Welding*, 1st Int'l Symposium on Friction Stir Welding, 1999, Thousand Oaks, USA.

[J06] N. Jemal, *Qualification du domaine de soudabilité en soudage par friction malaxage*, These, École Nationale Supérieure d'Arts et Métiers, 2011.

[K02] G. Karrar, A.N. Shuaib, F.A. Al-Badour, N. Merah, A.K. Mahgoub, *Friction stir butt welding of commercially pure copper plates*, Int'l Mechanical Engineering Congress and Exposition, IMECE 2014, Montreal, Canada.

[K03] H. Kasai, Y. Morisada, H. Fujii, *Dissimilar FSW of immiscible materials: Steel/magnesium*, Materials Science and Engineering 624 (2015) 250-255.

[K07] G. Kohn, Y. Greenberg, I. Makover, A. Munitz, *Laser-Assisted Friction Stir Welding*, American Welding Society 81 (2002) 46-48.

[L01] W.B. Lee, S.B. Jung, *The joint properties of copper by friction stir welding*, Materials Letters 58 (2004) 1041-1046.

[L02] C.M.A. Leitao, *Influence of base material plastic properties and process parameters on friction stir weldability*, Dissertation for the degree of Doctor of Philosophy in Mechanical Engineering, University of Coimbra, 2013.

[L03] W. Li, Z. Zhang, J. Li, Y.J. Chao, *Numerical Analysis of Joint Temperature Evolution During Friction Stir Welding Based on Sticking Contact*, J. of Materials Engineering and Performance 21(9) (2012) 1849-1856.

[L04] H.J. Liu, J.J. Shen, Y.X. Huang, L.Y. Kuang, C. Liu, C. Li, *Effect of tool rotation rate on microstructure and mechanical properties of friction stir welded copper*, Science and Technology of Welding and Joining 14(6) (2009) 577-583.

[L08] O. Lorrain, *Analyses expérimentale et numérique du procédé de soudage par friction malaxage FSW*, These, École Nationale Supérieure d'Arts et Métiers, 2010.

[M01] V.M. Magalhaes, C. Leitao, D.M. Rodrigues, *Friction stir welding industrialisation and research status*, Science and Technology of Welding and Joining 23 (2018) 400-409.

[M04] S. Mandal, J. Rice, A.A. Elmustafa, *Experimental and numerical investigation of the plunge stage in friction stir welding*, J. of Materials Processing Technology 203 (2007) 411-419.

[M05] K.P. Mehta, V.J. Badheka, *Hybrid approaches of assisted heating and cooling for friction stir welding of copper to aluminum joints*, J. of Materials Processing Technology 239 (2017) 336-345.

[M06] A. Meilinger, I. Török, *The importance of Friction Stir Welding Tool*, Production Processes and Systems 6 (2013) 25-34.

[M08] M. Milicic, P. Gladović, R. Bojanić, T.M. Savković, N. Stojic, *Friction stir welding (FSW) process of copper alloys*, Metalurgija 55(1) (2016) 107-110.

[M11] R.S. Mishra, Z.Y. Ma, *Friction stir welding and processing*, Materials Science and Engineering 50 (2005) 1-78.

[M12] R.S. Mishra, M.W. Mahoney, *Friction Stir Welding and Processing*, ASM Int'l, 2007.

[M13] P. Mitesh, D. Utsav, J. Mehul, *Effects of FSW on Mechanical properties and Microstructure of copper at Weld Joint*, Int'l J. of Engineering Development and Research 3(4) (2015).

[N02] R. Nandan, T. DebRoy, H.K.D.H. Bhadeshia, *Recent advances in friction-stir welding - process, weldment structure and properties*, Progress in Materials Science 53(6) (2008).

[N03] R. Negrea, R. Budişteanu, **M.A. Constantin**, C. Ducu, A.G. Plăiasu, S. Tabacu, S. Moga, D. Negrea, *Advanced Complementary Techniques for the Investigation of Pure Copper Plates Friction Stir Welding* (poster presentation), Annual Int'l Conference on Sustainable Development through Nuclear Research and Education, Nuclear 2018, 23.05.2018 Mioveni, România.

[N05] D.R. Ni, D.L. Chen, D. Wang, B.L. Xiao, Z.Y. Ma, *Tensile properties and strain-hardening behaviour of friction stir welded SiCp/AA2009 composite joints*, Materials Science and Engineering A 608 (2014) 1-10.

[O01] K. Okamoto, M. Doi, S. Hirano, K. Aota, H. Okamura, Y. Aono, T.C. Ping, *Fabrication of Backing Plates of Copper Alloy by Friction Stir Welding*, 3rd Int'l Friction Stir Welding Conference, 2001, Kobe, Japan.

[O02] K. Ozel, C. Cetinarslan, S.K. Genç, *Joining of Aluminum Alloys with Friction Stir Welding Method*, 3rd Int'l Conference on Recent Trends in Structural Materials, 2014, Pilsen, Czech Republic.

[P02] H. Pashazadeh, A. Masoumi, J. Teimournezhad, *Numerical modelling for the hardness evaluation of friction stir welded copper metals*, Materials and Design 49 (2013) 913-921.

[P03] H. Pashazadeh, J. Teimournezhad, A. Masoumi, *Numerical investigation on the mechanical, thermal, metallurgical and material flow characteristics in friction stir welding of copper sheets with experimental verification*, Materials and Design 55 (2014) 619-632.

[P05] P. Prasanna, S.B. Rao, M.K.G. Rao, *Finite element modeling for maximum temperature in friction stir welding and its validation*, Int'l J. of Advanced Manufacturing Technology 51(9) (2010) 925-933.

[R02] G. Rateau, *Méthode Arlequin pour les problèmes mécaniques multi-échelles: applications à des problèmes de jonction et de fissuration de structures élancées*, Ph.D. Thesis, École Centrale Paris, 2003.

[R03] ***, Rezumatul etapei a II-a (*Concepţie sistem de sudare. Concepţie sistem de monitorizare utilizând termografia în infraroşu*) a contractului 72174/2008, cu titlul "Dezvoltarea unor metode şi tehnici inovative de îmbinare a materialelor eterogene prin sudare prin frecare cu element activ rotitor", Institutul național de cercetare-dezvoltare în sudură și încercări de materiale - ISIM Timișoara.

[S01] P. Sahlot, A.K. Singh, V.J. Badheka, A. Arora, *Friction Stir Welding of Copper: Numerical Modeling and Validation*, Transactions of the Indian Institute of Metals 72 (2019) 1339-1347.

[S05] K. Savolainen, *Friction Stir Welding of Copper and Microstructure and Properties of the Welds*, Doctoral Thesis, Aalto University, 2012.

[S06] K. Savolainen, J. Mononen, H. Saukkonen, J. Koivula, *Friction Stir Weldability of Copper Alloys*, 5th Int'l Symposium on Friction Stir Welding, 2004, Metz, France.

[S10] D. Scirloi, **M.A. Constantin**, C. Badulescu, D. Negrea, M. Diakhate, E. Nitu, M. Iordache, *Influence des défauts de soudage FSW sur le comportement mécanique d'un assemblage bout à bout en Cu-DHP: analyse microscopique et par corrélation d'images numériques*, 24ème Congrès Français de Mécanique, CFM 2019, Brest, France *[Volum BDI]*.

[S11] E. Scutelnicu, D. Birsan, R. Cojocaru, *Research on Friction Stir Welding and Tungsten Inert Gas assisted Friction Stir Welding of Copper*, Recent Advances in Manufacturing Engineering (2011) 97-102.

[S12] J.J. Shen, H.J. Liu, F. Cui, *Effect of welding speed on microstructure and mechanical properties of friction stir welded copper*, Materials and Design 31 (2010) 3937-3942.

[S13] P. Sinclair, W. Longhurst, C. Cox, D. Lammlein, A. Strauss, G. Cook, *Heated Friction Stir Welding: An Experimental and Theoretical Investigation into how Preaheating Influences on Process Forces*, Materials and Manufacturing Processes 25 (2010) 1283-1291.

[S17] K. Surekha, A. Els-Botes, *Development of High Strength, High Conductivity Copper by Friction Stir Processing*, Materials and Design 32 (2011) 911-916.

[T02] W.M. Thomas, E.D. Nicholas, J.C. Needham, M.G. Murch, P. Temple-Smith, C.J. Dawes, Int'l Patent Application No. PCT/GB92/02203, GB Patent Application No. 9125978.8, US Patent Application No. 5.460.317, 1991.

[T04] D. Trimble, J. Monaghan, G.E. O'Donnell, *Force generation during friction stir welding of AA2024-T3*, Manufacturing Technology 61 (2012) 9-12.

[V02] ***, Vickers hardness tester, https://www.innovatest-europe.com/testing-knowledge/ (accessed on 20.07.2020).

[X01] G.M. Xie, Z.Y. Ma, L. Geng, *Development of a Fine-Grained Microstructure and the Properties of a Nugget Zone in Friction Stir Welded Pure Copper*, Scripta Materialia 57 (2007) 73-76.

[Y01] D.K. Yaduwanshi, S. Bag, S. Pal, *Numerical modeling and experimental investigation on plasma-assisted hybrid friction stir welding of dissimilar materials*, Materials and Design 92 (2016) 166-183.

[Z03] Y.N. Zhang, X. Cao, S. Larose, P. Wanjara, *Review of tools for friction stir welding and processing*, Canadian Metallurgical Quarterly 51 (2012).

[Z04] Z. Zhang, H.W. Zhang, *A fully coupled thermo-mechanical model of friction stir welding*, Int'l J. of Advanced Manufacturing Technology (2007) 279-293.

[Z07] X. Zhou, W. Pan, D. MacKenzie, *Identifying friction stir welding process parameters through coupled numerical and experimental analysis*, Int'l J. of Pressure Vessels and Piping 108-109 (2013) 2-6.

[Z08] S. Zimmer, *Contribution a l'industrialisation du soudage par friction malaxage*, These, École Nationale Supérieure d'Arts et Métiers, Spécialité "Génie Mécanique", 2009.